

**Figure 6.** Flow-cytometric scattergrams of KUSA-A1 cells (orange dots) and H-1/A cells (green dots) in the relationship between forward light scattering intensity and side light scattering intensity in the permeate solution after permeation of mixed cells of KUSA-A1 cells (orange dots) and H-1/A cells (green dots) through the PU membranes at (a) the cell density of each 50,000 cells/mL, and (b) following subsequent permeation of HSA solution. [Color figure can be viewed in the online issue, which is available at [www.interscience.wiley.com](http://www.interscience.wiley.com).]

Next the flow-cytometric analysis of the permeate solution of KUSA-A1 and H-1/A cells and also that of the recovery solution following filtration through PU membranes were examined. Figure 6(a) shows the forward versus side light scattering intensity in the permeate solution after permeation of the cells through PU membranes. Both smaller-sized KUSA-A1 and H-1/A cells passed through the PU membranes. Therefore, KUSA-A1 cells have a higher permeation ratio than H-1/A cells, because KUSA-A1 cells are typically smaller than H-1/A cells (see Figure 1).

Figure 6(b) shows the results of recovery solution following subsequent permeation of HSA solution. The pattern of the scattergram in the recovery solution [Figure 6(b)] was identical to that of the feed solution [Figure 1(b)], even though the numbers of both KUSA-A1 cells and H-1/A cells were significantly lower in the recovery solution. Thus, there is not a significant separation of KUSA-A1 and H-1/A cells in the recovery solution following permeation with HSA solution.

#### Cell Separation Through Various Porous Membranes

The separation of KUSA-A1 and H-1/A cells by several porous membranes, including uncoated nylon-net filters, fibronectin- or collagen-coated nylon-net filters, nonwoven fabrics made of acrylonitrile or a combination of nylon and polyester, silk screen No. 150 made of silk or Tetron™, and silk screen No. 250 made of Tetron™ were also examined. Figure 7 shows the permeation ratio through these membranes with the use of a feed solution containing a mixture of KUSA-A1 and H-1/A cells. With the use of the nylon-net filter and fibronectin-coated nylon-net filter, the permeation ratio for KUSA-A1 cells was higher than for H-1/A cells.

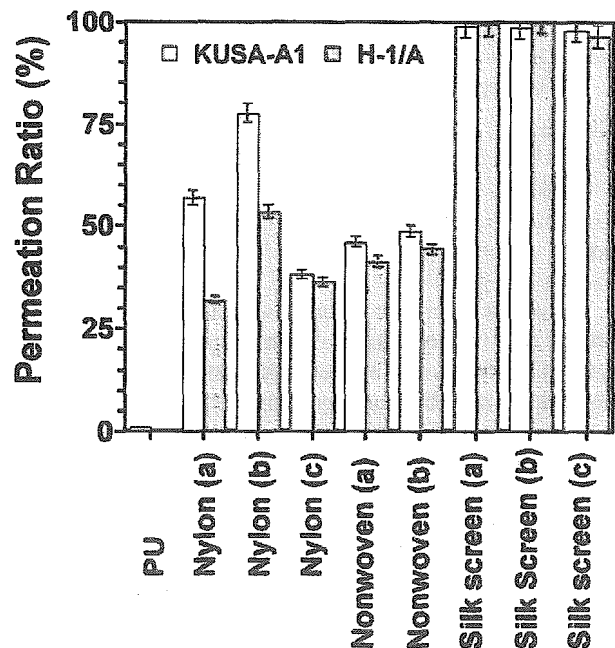


**Figure 7.** Permeation ratio of KUSA-A1 cells and H-1/A cells through PU, nylon-net filter [nylon (a)], nylon-net filter coated with fibronectin [nylon (b)] and collagen [nylon (c)], nonwoven fabrics made of acrylonitrile [nonwoven (a)], nylon and polyester [nonwoven (b)], and silk screens made of silk [silk screen (a), mesh size 150] and Tetron™ [silk screen (b), mesh size 150 and silk screen (c), mesh size 250] after permeation of mixed-cell solution at the cell density of 50,000 cells/mL and 25°C. Data are expressed as the means  $\pm$  standard deviation of four independent measurements.

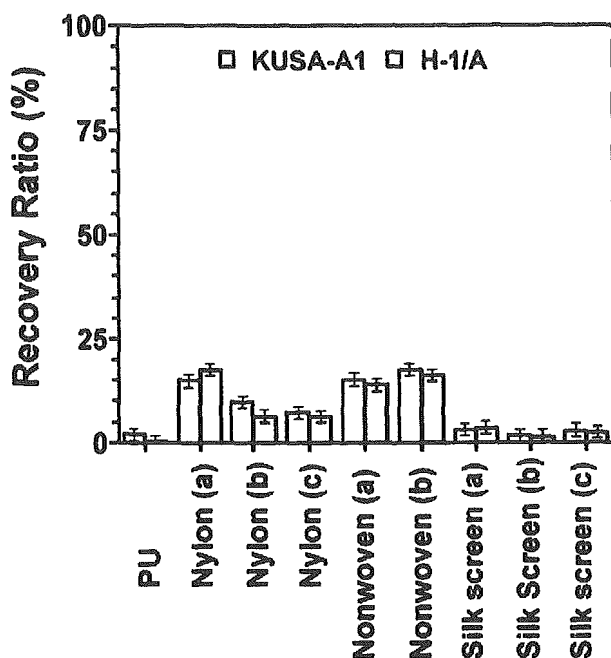


**Figure 8.** Recovery ratio of KUSA-A1 cells and H-1/A cells through PU, nylon-net filter [nylon (a)], nylon-net filter coated with fibronectin [nylon (b)] and collagen [nylon (c)], nonwoven fabrics made of acrylonitrile [nonwoven (a)], nylon and polyester [nonwoven (b)], and silk screens made of silk [silk screen (a), mesh size 150] and Tetron™ [silk screen (b), mesh size 150 and silk screen (c), mesh size 250] after permeation of mixed-cell solution at the cell density of 50,000 cells/mL and 25°C. Data are expressed as the means  $\pm$  standard deviation of four independent measurements.

This is mainly due to the smaller cell size of the KUSA-A1 cells as detected in the forward and side light scattering intensities shown in [Figure 1(b)]. In addition, a high cell permeation ratio was also found with the use of silk screens made of silk or Tetron™. This was because silk screens have a larger pore size than the nylon-net filter and PU membranes (see Figure 2). A relatively good separation factor for permeation ( $\alpha_p$ ), defined as the relative permeation ratio of KUSA-A1 cells divided by that of H-1/A cells, was obtained when the mixed-cell solution was passed through the nylon-net filter ( $\alpha_p = 1.8$ ) or fibronectin-coated nylon-net filter ( $\alpha_p = 1.5$ ) membranes, whereas a separation was not obtained when the nonwoven fabrics or silk screens were used. Overall, the results suggest that the pore size of nylon-net filter was optimal for producing a sieving effect.

The effect of passing the HSA solution through the porous polymeric membranes after permeation of the cell mixture was also assessed. As shown in Figure 8, the recovery ratio of both KUSA-A1 and H-1/A cells was relatively low (< 20%) for all of the membranes. This is caused by the high adhesiveness of the mesenchymal cells and their high permeation ratio. Analysis of the recovery solution shows that there was no effective separation of KUSA-A1 and H-1/A cells. This is probably due to the fact that the KUSA-A1 and H-1/A cells are both mesenchymal cells and have similar characteristics (i.e., adhesiveness).

## CONCLUSIONS

These results show that a separation of cells with similar characteristics, such as different types of mesenchymal cells (i.e., osteoblasts and preadipocytes) can be obtained in the permeate solution, but not in the recovery solution following membrane filtration. The main factor in this separation is the sieving effect of cells through the porous membranes. Therefore, prior to separation, flow cytometry should be carried out to confirm that the cells to be separated have different sizes. Separation factor, ( $\alpha_p = 1.8$ ) and a high permeation ratio was achieved when a mixed-cell solution was passed through a nylon-net filter with an 11- $\mu$ m pore size, whereas an extremely low permeation ratio (< 5%) of both cell types was found with the use of surface-modified or unmodified PU foaming membranes with a 12- $\mu$ m pore size. It was also found that the nylon-net filter had screen-like pore structure, whereas the PU membranes had a deformed open pore structure. This indicates that not only the pore size but also the pore morphology is important for membrane-based cell separation.

Even a small degree of enrichment, such as the separation factor of 1.8, is also considered effective in the transplantation of mesenchymal cells in clinical application, although clinical trials using the enriched-cell type of mesenchymal cells have not yet been performed. In conclusion, cell separation between mesenchymal progenitor cells through porous polymeric membranes was shown to be possible in this study. This technology will contribute to the future clinical application of cell transplantation into the damaged tissue of patients.

## REFERENCES

1. Umezawa A, Maruyama T, Segawa K, Shaddock RK, Waheed A, Hata J. Multipotent marrow stromal cell is able to induce hematopoiesis *in vivo*. *J Cell Physiol* 1992;151:197-205.
2. Kohyama J, Abe H, Shimazaki T, Koizumi A, Nakashima K, Gojo S, Taga T, Okano H, Hata J, Umezawa A. Brain from bone: Efficient "meta-differentiation" of marrow stroma-derived mature osteoblasts to neurons with Noggin or a demethylating agent. *Differentiation* 2001;68:235-244.
3. Edwards M, Twin J, Wilkinson S. New technique to assess the axilla for breast cancer metastases using cell separation technology. *Aust N Z J Surg* 2002;72:655-659.
4. Vij R, Brown R, Shenoy S, Haug JS, Kaesberg D, Adkins D, Goodnough LT, Khoury H, DiPersio J. Allogeneic peripheral blood stem cell transplantation following CD34<sup>+</sup> enrichment by density gradient separation. *Bone Marrow Transplant* 2000; 25:1223-1228.
5. Sanada Y. Transplantation of hematopoietic cells: General theory. In: Harada M, Katoh S, Sanada Y, editors. *New trends in hematopoietic stem cell transplantation*. Tokyo: Nanundo: 1998. p 1-7.
6. Gryn J, Shaddock RK, Lister J, Zeigler ZR, Raymond JM. Factors affecting purification of CD34<sup>+</sup> peripheral blood stem cells using the Baxter Isolex 300i. *J Hematother Stem Cell Res* 2002;11:719-730.
7. Carreras E, Saiz A, Marin P, Martinez C, Rovira M, Villamor N, Aymerich M, Lozano M, Fernandez-Aviles F, Urbano-Ispizua A, Montserrat E, Gaus F. CD34<sup>+</sup> selected autologous

- peripheral blood stem cell transplantation for multiple sclerosis: report of toxicity and treatment results at one year of follow-up in 15 patients. *Haematologica* 2003;88:306–314.
8. Domingo JC, Mercadal M, Petriz J, De Madariaga MA. Preparation of PEG-grafted immunomagneto liposomes entrapping citrate stabilized magnetite particles and their application in CD34<sup>+</sup> cell sorting. *J Microencapsul* 2001;18:41–54.
  9. Comella K, Nakamura M, Melnik K, Chosy J, Zborowski M, Cooper MA, Fehniger TA, Caligiuri MA, Chalmers JJ. Effects of antibody concentration on the separation of human natural killer cells in a commercial immunomagnetic separation system. *Cytometry* 2001;45:285–293.
  10. Kataoka K, Sakurai Y, Hanai T, Maruyama A, Tsuruta T. Immunoaffinity chromatography of lymphocyte subpopulations using *tert*-amine derived matrices with adsorbed antibodies. *Biomaterials* 1988;9:218–224.
  11. Ohba H, Bakalova R, Moriwaki S, Nakamura O. Fractionation of normal and leukemic T-cells by lectin-affinity column chromatography. *Cancer Lett* 2002;184:207–214.
  12. Komai H, Naito Y, Fujiwara K, Takagaki Y, Noguchi Y, Nishimura Y. The protective effect of a leucocyte removal filter on the lung in open-heart surgery for ventricular septal defect. *Perfusion* 1998;13:27–34.
  13. Muller-Steinhardt M, Hennig H, Kirchner H, Schlenke P. Prestorage WBC filtration of RBC units with soft-shell filters: filtration performance and impact on RBCs during storage for 42 days. *Transfusion* 2002;42:153–158.
  14. Higuchi A, Yamamiya S, Yoon BO, Sakurai N, Hara M. Peripheral blood cell separation through surface-modified polyurethane membranes. *J Biomed Mater Res* 2004;68:34–42.
  15. Kiyohara S, Sasaki M, Saito K, Sugita K, Sugo T. Radiation-induced grafting of phenylalanine-containing monomer onto a porous membrane. *Reactive Functional Polym* 1996;31:103–110.
  16. Kim M, Kiyohara S, Konishi S, Tsuneda S, Saito K, Sugo T. Ring-opening reaction of poly-GMA chain grafted onto a porous membrane. *J Membrane Sci* 1996;117:33–38.
  17. Higuchi A, Takanashi Y, Tsuzuki N, Asakura T, Cho CS, Akaike T, Hara M. Production of interferon- $\beta$  by fibroblast cells on membranes prepared with RGD-containing peptides. *J Biomed Mater Res* 2003;65:369–378.
  18. Higuchi A, Takanashi Y, Ohno T, Asakura T, Cho CS, Akaike T, Hara M. Production of interferon- $\beta$  by fibroblast cells on the membranes prepared by extracellular matrix proteins. *Cyto-technology* 2002;39:131–137.
  19. Higuchi A, Tamiya S, Tsubomura T, Katoh A, Cho CS, Akaike T, Hara M. Growth of L929 cells on polymeric films prepared by Langmuir-Blodgett and casting methods. *J Biomater Sci Polym Ed* 2000;11:149–168.
  20. Higuchi A, Shirano K, Harashima M, Yoon BO, Hara M, Hattori M, Imamura K. Chemically modified polysulfone hollow fibers with vinylpyrrolidone having improved blood compatibility. *Biomaterials* 2002;23:2659–2666.
  21. Keeney M, Chin-Yee I, Weir K, Popma J, Nayar R, Sutherland DR. Single platform flow cytometric absolute CD34<sup>+</sup> cell counts based on the ISAHE guidelines. *Cytometry* 1998;34:61–70.

Nobuyuki Kawashima · Kentaro Shindo · Kei Sakamoto  
Hisatomo Kondo · Akihiro Umezawa · Shohei Kasugai  
Bernard Perbal · Hideaki Suda · Minoru Takagi  
Ken-ichi Katsube

## Molecular and cell biological properties of mouse osteogenic mesenchymal progenitor cells, Kusa

Received: March 15, 2004 / Accepted: September 9, 2004

**Abstract** A cell line of murine osteogenic progenitor cells, Kusa, was established from femoral bone marrow stromal cells with other types of mesenchymal progenitor cells. We characterized two sublines of Kusa (Kusa-A1 and Kusa-O) from several aspects, including the use of an expression profiling system, a cDNA microarray. The original Kusa subline (Kusa-A1) had high alkaline phosphatase activity and high accumulation of calcium deposits in a condition inducing mineralization, with ascorbic acid and  $\beta$ -glycerophosphate. Kusa-O, a low osteogenic subline of Kusa, had high alkaline phosphatase activity but slow accumulation of calcium deposits even in the inducing condition. These two Kusa sublines differed in the expression of the osteogenic marker genes, *osteocalcin* and *osteopontin*, during mineralization. A type of cDNA microarray revealed marked downregulation of gene expression in the inducing condition in both Kusa-A1 and Kusa-O. Another type of

high-throughput microarray was performed to examine the difference in gene expression patterns between Kusa-A1 and Kusa-O. By this analysis, *periostin*, which would be involved in a stage of osteogenesis, was low in Kusa-A1. On the contrary, *Myocyte enhancer factor 2C (MEF2C)*, a myogenic transcriptional factor, was high in Kusa-A1, although no expression of any other myogenic genes was shown.

**Key words** Osteogenesis · Stem cells · Notch · MEF2 · Periostin

### Introduction

The ability of mesenchymal progenitor cells to differentiate has been the subject of a growing body of documents that have revealed the unexpected potential of bone marrow cells [1,2]. Bone marrow stromal cells support the growth and differentiation of hematopoietic stem cells by both direct and indirect influences [3], and they themselves can differentiate into various types of cells, i.e., striated muscle [4], heart muscle [5], bone tissue [6], chondrocytes [7], and even neurons [8] or hepatocytes [9]. However, few studies have been done about the molecular basis of their potential, and this potential is a puzzle, considering their paradoxical stability (cells that have pluripotency but keep the quiescent state in situ) [7,10]. Further more, bone marrow progenitor cells were demonstrated to be involved in the recovery of blood vessel injury, although they caused atherosclerosis [11]. Thus, it seems that mesenchymal progenitor cells sometimes generate pathogenic change, and it is necessary to investigate their activity from a non-restitutive aspect.

The factors that regulate the potential of mesenchymal progenitor cells have been investigated in various ways. Among them, myogenesis was well-examined at a molecular level, using C3H10T1/2, a murine pluripotent fibroblastic cell line. The discovery of *MyoD* was a turning point in myogenesis research [12] and the *MyoD* gene family is now believed to control the major path of myogenesis [13].

N. Kawashima (✉) · K. Shindo · H. Suda  
Pulp Biology and Endodontics, Graduate School of Tokyo Medical and Dental University, 1-5-45 Yushima, Bunkyo-ku,  
Tokyo 113-8549, Japan  
Tel./Fax +81-3-5803-5494  
e-mail: kawashima.n.endo@tmd.ac.jp

N. Kawashima  
Center of Excellence Program for Research on Molecular Destruction and Reconstruction of Tooth and Bone, Graduate School of Tokyo Medical and Dental University, Tokyo, Japan

A. Umezawa  
Department of Reproductive Biology and Pathology, National Institute for Child Health and Development, Tokyo, Japan

B. Perbal  
Laboratoire d'Oncologie Virale et Moléculaire, UFR de Biochimie, Université Paris, Paris, France

K. Sakamoto · M. Takagi · K. Katsube  
Molecular Pathology, Graduate School of Tokyo Medical and Dental University, Tokyo, Japan

H. Kondo · S. Kasugai  
Masticatory Function Control, Graduate School of Tokyo Medical and Dental University, Tokyo, Japan

N. Kawashima and K. Katsube contributed equally to this work

Adipogenesis was also investigated using the same cell line, and *peroxisome proliferator-activated receptor gamma* (*PPAR gamma*), a receptor of prostaglandin, was demonstrated to control the adipogenesis [14]. Compared with these investigations of myogenesis, little is known about osteogenesis and chondrogenesis. In 1997, a member of the RUNX family, CBFA1 (RUNX2) was demonstrated to be involved in osteogenesis, in a study of a null mutant mouse [15]. Recently, a type of zinc finger protein, called "osterix", was also reported to be involved in osteogenesis [16]. But the commitment of these transcriptional factors was not enough to initiate osteogenesis. Some other factors seem to be involved, but systematic investigation has not yet been done. One of the reasons might be that the cells used for such studies, e.g., primary cultures of osteoblasts or osteosarcoma cell lines, had inadequate capacity for bone formation [17,18].

Umezawa et al. [6] in experiments attempting the immortalization of murine bone marrow stromal cells, succeeded in the establishment of several mesenchymal progenitor cell lines (KUMs). One of them, named "Kusa", was unique in that it had osteogenesis potential in vivo. We investigated this cell line from the molecular aspect, including the use of cDNA microarray, to analyze the global dynamics of its gene expression pattern (gene profiling) [1,19].

## Materials and methods

### Cell culture

Kusa was established from mouse bone marrow stromal cells. Briefly, eluted stromal cells from the femoral bone marrow were transferred to a Dexter-type long-term culture [6]. Limiting dilution and continuous passage were performed to isolate the monoclonal cell populations. Various types of cell line were identified (KUMs) and one of them, named "Kusa", was found to possess osteoblastic properties in vivo. Five independent sublines were established from the in vivo cell mass of Kusa, after in vitro culture with limiting dilution. One of them, Kusa-A1, was selected for its particularly high osteogenic activity, and another subline, Kusa-O, was identified as non-osteogenic, although it had high alkaline phosphatase (ALP) activity. Kusa-A1 and Kusa-O were cultured in  $\alpha$ -modified minimum essential medium containing 10% fetal calf serum. Cells were inoculated at 5000 cells/cm<sup>2</sup> and incubated until confluency for passage. Mineralization was induced by adding 0.2 mM ascorbic acid and 5 mM  $\beta$ -glycerophosphate to the same medium after confluency (inducing condition) [20,21].

### Measurement of alkaline phosphatase (ALP) activity and calcium content

Alkaline phosphatase (ALP) activity was measured with an ALP measurement kit, (ALP-K Test, Wako Chemicals,

Tokyo, Japan). The accumulation of calcium deposits was measured with a calcium measuring kit, Ca-E Test (Wako Chemicals), using the cell extracts treated with HCl. To determine these two activities in the cell population, normalization was performed by measuring the protein concentration in extracts. The protein concentration was measured with a DC Protein assay kit (Bio-Rad, Hercules, CA, USA). All measurements were performed by independent triplicate studies.

### Northern blot and reverse transcription-quantitative reverse transcription (RT)-quantitative polymerase chain reaction (qPCR) analysis

Total RNA was extracted and purified with TRIzol (Invitrogen, Carlsbad, CA, USA). Ten micrograms of total RNA was applied to each lane of 1.2% formaldehyde agarose gel and electrophoresed. The RNA was transferred to a Nylon membrane (HybondN+; Amersham Biosciences, Piscataway, NJ, USA) and hybridized to <sup>32</sup>P-labeled DNA probes. Signals were detected and measured with a digital image analyzer, BAS-2500 (Fuji Photo Film, Tokyo, Japan). Labeled cDNA probes were made using a 488-bp fragment of mouse *Osteocalcin* (*OC*) cDNA (provided by J. Wozney [Celeste et al. [22]), a 984-bp fragment of mouse *Osteopontin* (*OPN*) cDNA (provided by Nomura et al. [23]), a 2673-bp fragment of mouse *Notch1* intracellular domain cDNA (provided by J. Nye), a 1609-bp fragment of rat *HES1* cDNA (provided by R. Kageyama), and a 2380-bp fragment of mouse *CCN3 nephroblastoma overexpressed gene* (*Nov*), cloned by B. Perbal. The qPCR was performed (DyNAmo, DNA engine Opticon; MJ Japan, Tokyo, Japan) with the first-strand cDNA synthesized from 500 ng of total RNA (SuperScript II; Invitrogen). The primer sequences were as follows: MEF2C (141 bp): 5'-ATGGA TGAGCGTAACAGACAGGTG-3' and 5'-CGTTGTAC TCGGTGTA CTTGAGCA-3'; periostin (100 bp): 5'-ACC CTGCAAATGCCAACAGT-3' and 5'-AGAATTTGCT GGAGGGCACA-3'; and  $\beta$ actin (380 bp): 5'-TCGGTCA GGATCTTCATGAG-3' and 5'-AGTACCCCATTGAA CATGGC-3'.

### cDNA array analysis

Global examination of gene expression was performed with a cDNA gene expression array (Atlas mouse cDNA Expression Array; BD Biosciences Clontech, Palo Alto, CA, USA). This microarray carries 588 mouse cDNAs for general profiling. The complete list of cDNAs is available at the website of Clontech (<http://www.clontech.com>). The extracted total RNA was eluted through an oligo-dT cellulose (Amersham Sciences, Piscataway, NJ, USA) column to purify polyA mRNA. cDNA probes were made from the poly A mRNA, following the manufacturer's protocol, with the specific primers and [ $\alpha$ -<sup>32</sup>P] dATP and hybridized to the array membrane. Signals were detected and measured with a digital image analyzer (BAS-2500).

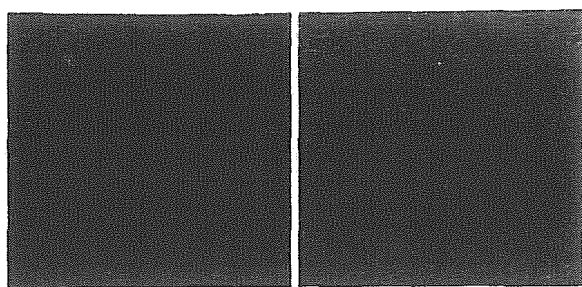


**Fig. 1.** Phase contact photomicrographs of Kusa-A1 and Kusa-O. Morphologically, Kusa-A1 (A) and Kusa-O (B) were similar, with a spindle or polygonal shape. Kusa-O was slightly larger than Kusa-A1 in cell size. Bar represents 100  $\mu\text{m}$

Another microarray analysis was done with the GEMarray (Incyte/Genome Systems, Palo Alto, CA, USA). This microarray was based on a fluorescence labeled (Cy3 and Cy5) cDNA probe to distinguish the two sources. Hybridization on the slide glasses and image analysis were done by the company. The results were expressed in reference to the GenBank addresses.

## Results

### Morphological properties of Kusa

Before confluence, Kusa-A1 had a fibroblastic appearance, with a polygonal flat or spindle shape (Fig. 1A). Kusa-O was slightly larger than Kusa-A1 in cell size (Fig. 1B), although no significant difference was observed. Kusa did not exhibit tumor-cell-like growth, such as piling up, nor did it form a focus in normal medium (non-inducing condition). On treatment with ascorbic acid and  $\beta$ -glycerophosphate (inducing condition), Kusa-A1 exhibited mineralization (Fig. 2). Kusa-A1 gradually accumulated extracellular matrices as small sandy precipitates that covered the surface of cell aggregates. The accumulation was positively stained with Alizarin Red S. These nodules were visible on day 3 and showed condensed staining on day 5 (Fig. 2B,C). In the non-inducing condition, Kusa-A1 spontaneously exhibited nodule-like structures on day 5, although the nodules were rather small and not stained with Alizarin Red S (Fig. 2A). Kusa-O did not exhibit rapid mineralization. In the inducing condition, mineralized nodules were gradually accumulated from day 10 (Fig. 2E,F,G). The Alizarin Red S-positive spots in Kusa-O were rather large but diffuse, and their margins were not clear, as compared with the nodule margins in Kusa-A1. In the non-inducing condition, Kusa-O formed nodules, but they were rather small and not stained with Alizarin Red S (Fig. 2D). High magnification of the Kusa-A1 culture stained with Alizarin Red S showed that the calcified area appeared like "spots", distinctly separate from the non-calcified area (Fig. 2H). The calcified area in Kusa-O showed obscure margins and non-condensed stain (Fig. 2I).

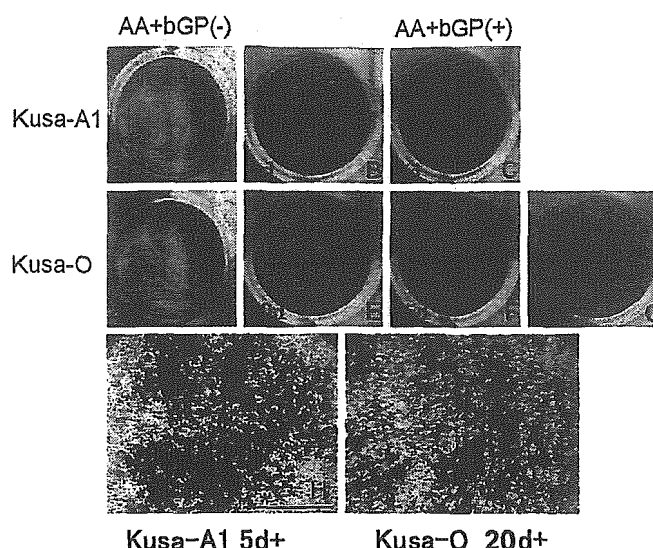


**Fig. 2.** Mineralized nodule formation in Kusa-A1 and Kusa-O. Mineralized nodules were detected by Alizarin Red S staining. Kusa-A1 cultured in the non-inducing condition (without ascorbic acid [AA] and  $\beta$ -glycerophosphate [ $\beta$ GP; AA +  $\beta$ GP(-)] did not form mineralized nodules 5 days (d) after confluency (A), but in the inducing condition (addition of AA and  $\beta$ GP AA +  $\beta$ GP(+)) these nodules were formed on day 3 (B), and nodules showing condensed staining were formed on day 5 (C). Kusa-O did not form mineralized nodules 20 days after confluency in the non-inducing condition (D), but, in the inducing condition, formed them on day 10 (E); the nodules then developed moderately (F day 15; G day 20). H and I show high-magnification views of mineralized nodules. H In Kusa-A1, the nodules had a discrete margin (asterisks indicating the development of "salt-and-pepper pattern"-like dot structures, but in Kusa-O (I), the margins of the nodules were ambiguous. Bar represents 500  $\mu\text{m}$ . A-G  $\times 1$

### Calcium accumulation

Kusa-A1 and Kusa-O apparently differed in calcium accumulation rates (Fig. 3). In the non-inducing condition, neither Kusa-A1 nor Kusa-O exhibited calcium accumulation until day 5. However, Kusa-A1 showed marked accumulation of calcium deposits in the inducing condition. On day 5, the calcium level was 20-fold higher than that in the initial state. Kusa-O was not reactive to the inducing condition and showed little change even on day 5. MC3T3-E1 cells (a mouse osteoblastic cell line) did not show apparent accumulation of calcium deposits during the time course.

### ALP activity and insoluble calcium content

Kusa-A1 had extraordinarily high ALP activity (0.8 IU/mg) even before mineralization, and this activity was constant both in the inducing and the non-inducing conditions (Fig. 3). The very high ALP activity of Kusa-A1 was marked as compared with that in MC3T3-E1, which had 20-fold less ALP activity than Kusa-A1. Kusa-O had relatively low ALP activity at the beginning (though it was much higher than that in MC3T3-E1), but the activity gradually increased in the inducing condition, to 1.2 IU/mg on day 5.

**Fig. 3.** Calcium accumulation and alkaline phosphatase (ALP) activity in Kusa-A1 and Kusa-O. Calcium accumulation was observed only in Kusa-A1 on day 5 after confluency in the inducing condition (Kusa-A1+). High ALP activity was observed in Kusa-A1 in the non-inducing condition (Kusa-A1-) and ALP was rather low in the inducing condition (Kusa-A1+). ALP activity in Kusa-O was not high at the beginning, but was gradually upregulated during the time course in the non-inducing condition (Kusa-O-) and the inducing condition accelerated this upregulation (Kusa-O+). ALP activity in MC3T3-E1 was much lower than that in Kusa-A1 and Kusa-O. MC3T3-E1 was cultured in both inducing and non-inducing conditions. Minus sign “-” indicates the absence of AA and  $\beta$ GP and “+” indicates the presence of AA and  $\beta$ GP

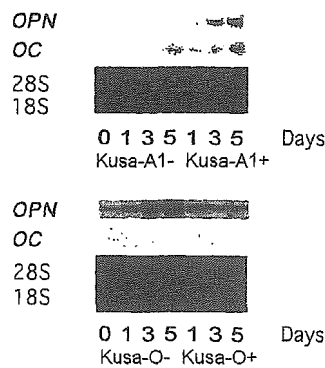
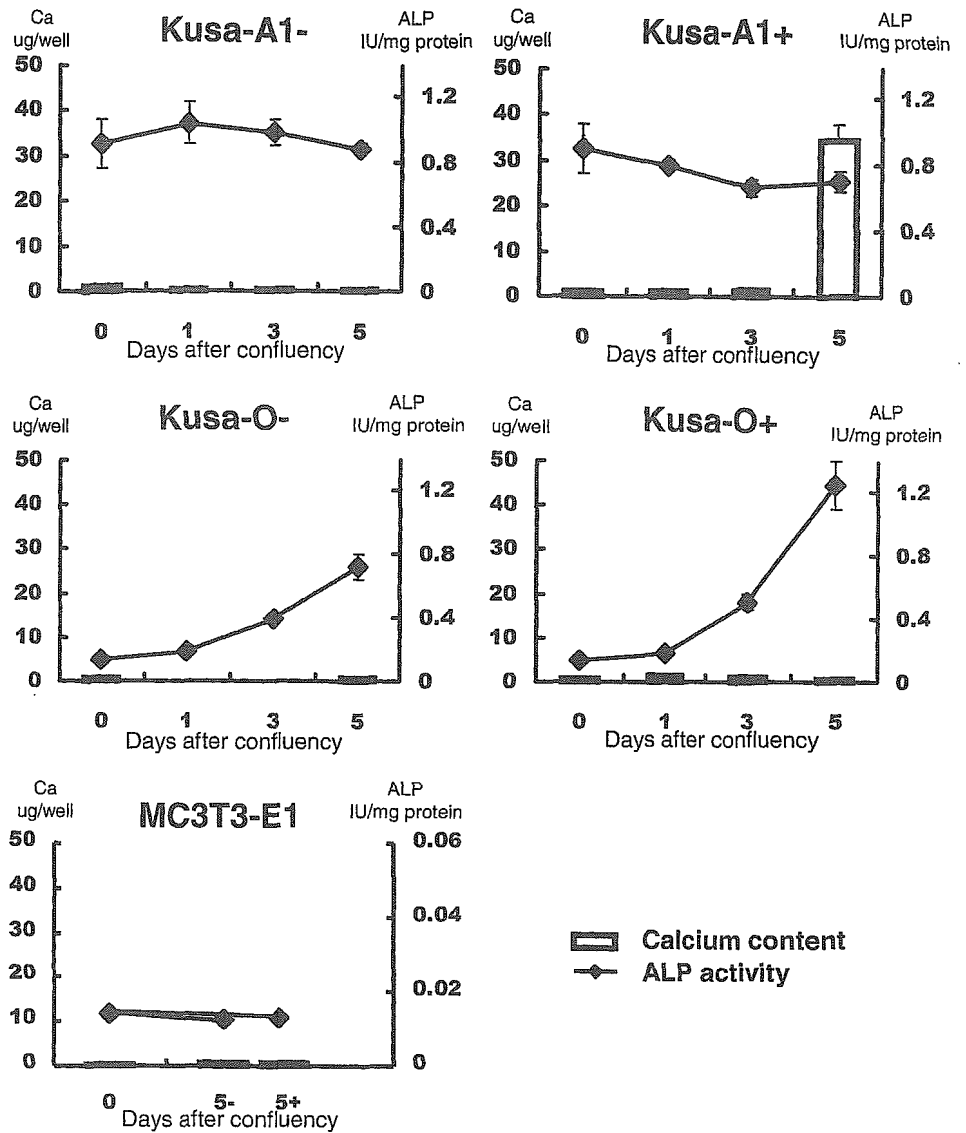


**Fig. 4.** Osteocalcin (OC) and Osteopontin (OPN) expression in Kusa-A1 and Kusa-O. In Kusa-A1, Osteocalcin expression was observed on day 5 in the non-inducing condition, and was seen on day 1 in the inducing condition. Its expression was gradually upregulated in the time course. In contrast, Kusa-O did not express Osteocalcin. Osteopontin expression was high only in the inducing condition in Kusa-A1, but its expression was observed in both conditions in Kusa-O. Minus sign “(-)” indicates the absence of AA and  $\beta$ GP and + indicates the presence of AA and  $\beta$ GP

Expression of osteogenic marker genes

We examined two osteogenic markers, *osteopontin* (OPN) and *osteocalcin* (OC) (Fig. 4). In Kusa-A1, *osteopontin* expression was not detectable in the non-inducing condition, although *Osteocalcin* was slightly upregulated. In the inducing condition, *osteocalcin* expression was high from day 1 and gradually increased. *Osteopontin* expression was gradually upregulated in the inducing condition. Kusa-O showed a relatively constant level of *osteopontin* expression in the inducing condition, whereas the level was high in the non-inducing condition. *Osteocalcin* expression was not detectable in Kusa-O in either the inducing or the non-inducing condition.

Expression of Notch signal genes

To examine the properties of Kusa as stem cells, genes related to the Notch signal were investigated (Fig. 5). The



Fig. 5. Notch signal expression in *Kusa-A1* and *Kusa-O*. Top row, *Notch1*; middle row, *CCN3* (*Nov*); bottom row, *HES1*. Minus sign (–) indicates the absence of AA and  $\beta$ GP and + indicates the presence of AA and  $\beta$ GP

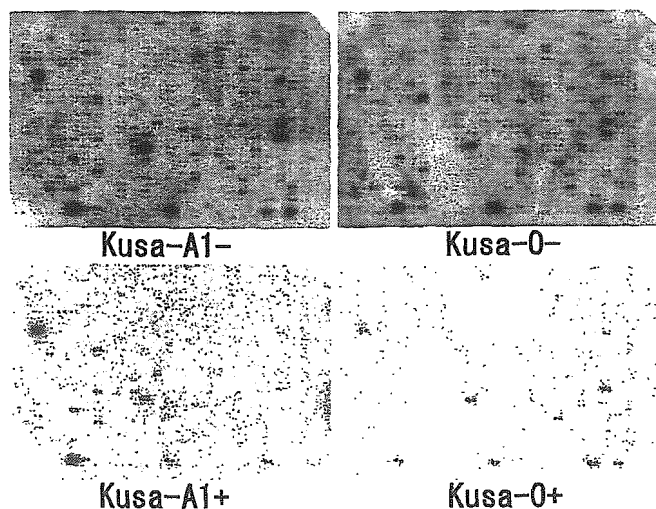


Fig. 6. Atlas Microarray (Clontech) surveillance of *Kusa-A1* and *Kusa-O* in both the non-inducing and the inducing conditions. The profile of *Kusa-A1* was generally similar to that of *Kusa-O*. The inducing condition showed a marked downregulation of gene expression in both cell lines. Minus sign (–) indicates the absence of AA and  $\beta$ GP and + indicates the presence of AA and  $\beta$ GP

Notch signal is fundamental for the regulation of stem cells, and *CCN3* is a regulator of the Notch signal whose expression is often found in mesenchymal cells. *CCN3* expression was discrete in both *Kusa-A1* and *Kusa-O*. In *Kusa-A1*, it was high in the non-inducing condition. *Notch1* expression in *Kusa-A1* was observed in the non-inducing condition. Weak *Notch1* expression was observed on day 3 in the inducing condition in both *Kusa-A1* and *Kusa-O*. *HES1* expression in *Kusa-A1* was transiently upregulated in the non-inducing condition. In *Kusa-O*, *HES1* expression was not observed. In conclusion, subtle differences were observed in the expression patterns of the examined genes related to the Notch signal.

#### Gene expression profile, using cDNA microarray

To clarify the differences in gene expression in *Kusa-A1* and *Kusa-O* in detail, global examination was done using microarray methods. We performed cDNA array analysis of 588 genes with the Atlas Mouse cDNA Expression Array (Clontech) (Fig. 6) in both the inducing and non-inducing

conditions. From an overview of the hybridization image, it was clear that global downregulation occurred in the inducing condition in both *Kusa-A1* and *Kusa-O*. In the non-inducing condition, about 140 genes were expressed in the panel, and in the inducing condition, about 50 genes (including several housekeeping genes) were expressed. In about 50 remaining genes, no genes directly involved in osteogenesis were found (Table 1). However, several genes possibly related to osteogenesis (Table 1) showed differences between the cell lines. For *Kusa-A1*, *ski* and *TIMP 2* and *3* were upregulated in the inducing condition. In contrast, *MAPKK1* and *TGF $\beta$ 2* were upregulated for *Kusa-O*.

To compare the expression patterns between *Kusa-A1* and *Kusa-O*, another type of microarray, (GEMarray; Incite/Genome Systems) was carried out, which could analyze more than 8000 clones. Several genes (clones) that showed great differences in expression were demonstrated (Tables 2 and 3) though they did not include known genes directly related to osteogenesis. Tables 2 and 3 show that *myocyte enhancer factor 2C* (*MEF2C*) is a gene that was highly expressed in *Kusa-A1*. This gene is regulated principally by other myogenic transcriptional factors, such as *MyoD* and *Myf5*, but the GEMarray analysis did not show upregulation of any other myogenic markers. The expression rate of *MEF2C* was also confirmed by qRT-PCR (Fig. 7). In contrast to the expression of *MEF2C* in *Kusa-O*, *periostin* (also known as *osteoblast-specific factor-2* [*OSF-2*]) was high in *Kusa-O* (Fig. 7). The role of this fasciclin 1-like extracellular protein has not yet been clarified, but it may play a role in the recruitment and attachment of osteoblast precursors in the periosteum [24].

#### Discussion

We investigated the properties of an osteogenic cell line, *Kusa*, from several aspects. This cell line has unidirectional potential for osteogenesis/mineralization in the normal condition and was classified into two sublines, *Kusa-A1* and *Kusa-O*, by mineralization activity. *Kusa-A1* had high ability for osteogenesis/mineralization in vivo and in vitro. The osteogenic ability of *Kusa-A1* was remarkable; it showed mineralization within 5 days in the inducing condition, whereas a well-known mouse osteoblastic cell line, MC3T3-E1, first demonstrated mineralized nodules only on day 20 (personal data). *Kusa-O* was relatively slow to show mineralization as compared with *Kusa-A1*, but it is not appropriate to call it “non-osteogenic”, because its activity was almost the same as that of MC3T3-E1. Both *Kusa* sublines should be categorized as high osteogenic cell lines.

The high ALP activity of *Kusa* was remarkable when compared with that of the osteogenic cell line MC3T3-E1. The constant high ALP activity in *Kusa-A1* may have influenced its strong mineralization ability, and the progressive upregulation of ALP in *Kusa-O* would explain its slow mineralization. Calcium deposition was faster in *Kusa-A1* than in *Kusa-O* in the inducing condition, but in the



Table 1. Atlas mouse cDNA expression array (Clontech) results

Experimental		Control		Ratio	Difference	UP	DOWN	Gene	Genbank no.
A1-	VS	O-	O-						
Spot Intensity									
Coordinate	O-	A1-	O-	Ratio	Difference	UP	DOWN	Gene	Genbank no.
D4k	0	7830	-7830	N/C		UP		Interferon inducible protein 1	U19119
D3l	194	5724	-5530	29.51		UP		HMG-box transcription factor from testis (MusSox17)	D49474
F7n	1312	12118	-10806	9.24		UP		Tissue inhibitor of metalloproteinases 3 (TIMP3); SUN	L19622
F7m	1538	7758	-6220	5.04		UP		Tissue inhibitor of metalloproteinases 2 (TIMP2)	X62622
C3h	2237	10392	-8155	4.65		UP		FLICE-like inhibitory protein long form (FLIP-L)	U97076
A4g	1301	5912	-4611	4.54		UP		Ski protooncogene	U14173
A7m	20965	12092	8873	0.58			DOWN	Prothymosin alpha (PTMA)	X56135
B1b	8176	4402	3774	0.54			DOWN	HSP60	X53584
B1d	11509	5186	6323	0.45			DOWN	HSP86; heat shock 86-kDa protein	M36830
F4g	11315	5012	6303	0.44			DOWN	Transforming growth factor beta 2 precursor (TGF-beta 2)	X57413
A1c	6224	2730	3494	0.44			DOWN	Breast cancer type 2 susceptibility protein (BRCA2)	U65594
C1m	7286	3096	4190	0.42			DOWN	Glutathione reductase	X76341
F7a	12115	4714	7401	0.39			DOWN	Interleukin-converting enzyme (ICE)	L28095
B6a	13899	4406	9493	0.32			DOWN	MAP kinase kinase 1	L02526
Spot Intensity									
Coordinate	A1-	A1+	Difference	Ratio	Difference	UP	DOWN	Gene	Genbank no.
A1g	9784	997	-8787	9.81		UP	DOWN	Mothers against dpp protein 1 (msMAD1; mSMAD1; MADH1); TGF-beta signaling protein 1 (BSP1)	U58992
B4a	8622	890	-7732	9.69			DOWN	NF-kappa-B transcription factor p65 subunit (NF-kB p65); relA; NFKB3	M61909
E3d	12134	1415	-10719	8.58			DOWN	Interleukin-3 receptor	M29855
E3h	5924	1014	-4910	5.84			DOWN	Interleukin-8 receptor	D17630
F3k	9742	1860	-7882	5.24			DOWN	7S Nerve growth factor alpha subunit (alpha-NGF; NGFA); KLIK4	M11434

F71	12804	2914	4.39	-9890	DOWN	47-kDa Heat shock protein precursor (HSP47); collagen-binding protein 1 (CBP1); serine protease inhibitor J6	J05609
		O+	V/S	O-			
E3f	23780	6790	3.50	-16990	DOWN	Interleukin-5 receptor alpha subunit precursor (IL-5R alpha)	D90205
C3h	10392	3185	3.26	-7207	DOWN	FLICE-like inhibitory protein long form (FLIP-L)	U97076
D3i	6392	2700	2.37	-3692	DOWN	HMG-box transcription factor from testis (MusSox17)	D49474
F7n	12118	5446	2.23	-6672	DOWN	Tissue inhibitor of metalloproteinases 3 (TIMP3); SUN	L19622
B5i	1182	4778	0.25	3596	UP	58-kDa Inhibitor of RNA-activated protein kinase	U28423
D6h	1500	7089	0.21	5589	UP	T-Lymphocyte activated protein	M31042
C2e	424	4561	0.09	4137	UP	Tumor necrosis factor alpha-induced protein 3 (TNFAIP3); TNFIP3; A20 zinc finger protein	U19463
Spot intensity							
Coordinate	O-	O+	Ratio	Difference	UP	Gene	Genbank no.
D5m	8545	0	N/C	-8545	DOWN	Split hand/foot gene	U41626
D6n	7025	0	N/C	-7025	DOWN	cAMP-Dependent transcription factor 3 (ATF3); activating factor 3; transcription factor LRG-21	U19118
D6m	5215	0	N/C	-5215	DOWN	Transcription factor LIM-1	Z27410
B1d	7205	864	8.34	-6341	DOWN	HSP86; heat shock 86-kDa protein	M36830
B4a	5790	874	6.62	-4916	DOWN	NF-kappa-B transcription factor p65 subunit (NF-kB p65); relA; NFKB3	M61909
F7i	6700	2020	3.32	-4680	DOWN	47-kDa Heat shock protein precursor (HSP47); collagen-binding protein 1 (CBP1); serine protease inhibitor J6	J05609
B6a	8700	2786	3.12	-5914	DOWN	Dual-specificity mitogen-activated protein kinase kinase 1 (MAP kinase kinase 1; MAPK kinase 1; MAPKK1); erk activator kinase 1 (MEK1); PRKMK1	L02526
F7a	7584	2460	3.08	-5124	DOWN	Interleukin-converting enzyme (ICE)	L28095
D1n	1628	9729	0.17	8101	UP	Sim transcription factor	U42554
B5i	1182	7497	0.16	6315	UP	58-kDa Inhibitor of RNA-activated protein kinase	U28423
F7d	1093	8084	0.14	6991	UP	Protease nexin 1 (PN-1)	X70296
D6m	0	8331	0.00	8331	UP	Transcription factor LIM-1	Z27410

The ratio of each pair was calculated with signal intensity, and if the ratio was more than 1.67 or less than 0.6, the spotted genes were considered to be upregulated or downregulated, respectively. Minus sign (-) indicates the absence of AA and  $\beta$ GP and (+) indicates the presence of AA and  $\beta$ GP.

**Table 2.** Mouse GEM array (Incite/Genome Systems) results: sorted by balanced differential expression in descending order

Differential expression	Kusa-A1 signal	Kusa-O signal	Gene name
5.1	18153	3573	Tissue inhibitor of metalloproteinase 3 (IMAGE:580753)
4.4	2254	516	Myocyte enhancer factor 2C (IMAGE:777101)
3.8	6829	1778	Alkaline phosphatase 2, liver (IMAGE:535409)
3.6	1963	542	ESTs (IMAGE:735883)
3.3	12133	3631	Tenascin C (IMAGE:736372)
3.3	803	241	<i>Mus musculus</i> neural precursor cell expressed developmentally; downregulated Nedd9 (Nedd9) mRNA, complete cds (IMAGE:404536)
2.9	15184	5181	Procollagen, type V, alpha 2 (IMAGE:467107)
2.8	8897	3222	Procollagen, type V, alpha 2 (IMAGE:445075)
2.6	1071	409	ESTs (IMAGE:597280)
2.5	3927	1544	ESTs (IMAGE:419146)
2.5	1683	667	ESTs (IMAGE:479709) <sup>a</sup>
2.4	5265	2152	Procollagen, type XI, alpha 1 (IMAGE:423028)
2.4	2616	1069	Public domain EST (IMAGE:597342)
2.3	6241	2702	Public domain EST (IMAGE:439362)
2.3	1737	749	Kinesin family member 5B (IMAGE:760837)
2.3	829	362	<i>Mus musculus</i> major histocompatibility complex region NG27, NG28, RPS28, NADH oxidoreductase, NG29, KIFC1, Fas-binding protein, BING1, tapasin, RalGDS-like, KE2, BING4, beta 1,3-galactosyl transferase, and RPS18 genes, complete cds (IMAGE:329741)
2.3	2778	1226	Sprouty homolog 1 ( <i>Drosophila</i> ) (IMAGE:425005)
2.2	2866	1314	ESTs (IMAGE:466255)
2.2	2214	1006	ESTs, weakly similar to plexin 1 ( <i>M.musculus</i> ) (IMAGE:735903)
2.2	1339	609	Adducin 3 (gamma) (IMAGE:620815)
2.2	5249	2434	Alkaline phosphatase 2, liver (IMAGE:465052)

<sup>a</sup>IMAGE:479709 clone was similar to *Mus musculus* MADS box transcription enhancer factor 2, polypeptide C (myocyte enhancer factor 2C)

**Table 3.** Mouse GEM array (Incite/Genome Systems) results: sorted by balanced differential expression in ascending order

Differential expression	Kusa-A1 signal	Kusa-O signal	Gene name
-5.3	951	5080	Stromal cell-derived factor 1 (IMAGE:533003)
-4.5	205	929	ESTs (IMAGE:779168)
-4.5	156	708	ESTs, weakly similar to cDNA EST EMBL:D75506 comes from this gene ( <i>C.elegans</i> ) (IMAGE:334182)
-4.4	220	963	ESTs (IMAGE:445426)
-4	1303	5260	Secreted phosphoprotein 1 (IMAGE:571759)
-3.9	362	1408	Four and a half LIM domains 1 (IMAGE:477066)
-3.7	456	1671	Fibrillin 2 (IMAGE:617885)
-3.7	218	809	Complement component 1, r subcomponent (IMAGE:617816)
-3.6	830	3021	<i>Mus musculus</i> OSF-2/periostin mRNA, complete cds (IMAGE:403071) <sup>a</sup>
-3.4	1204	4149	ESTs (IMAGE:617992)
-3.3	324	1060	Complement component 1 subcomponent (IMAGE:676176)
-3	507	1535	Calpain 6 (IMAGE:478504)
-2.9	812	2315	<i>Mus musculus</i> mRNA for dickkopf-3 (dkk-3 gene) (IMAGE:536577)
-2.8	1076	3010	Phosphodiesterase 7A (IMAGE:314384)
-2.8	366	1007	Public domain EST (IMAGE:314509)
-2.7	731	1939	ESTs (IMAGE:536526)
-2.6	1044	2672	Chloride channel 2 (IMAGE:407704)
-2.6	291	768	ESTs, weakly similar to proline-rich protein MP4 ( <i>M.musculus</i> ) (IMAGE:458992)
-2.6	274	708	Insulin-like growth factor 1 (IMAGE:313322)
-2.5	2177	5462	ESTs, weakly similar to similarity to yeast D-lactate dehydrogenase ( <i>C.elegans</i> ) (IMAGE:748228)
-2.5	280	693	Public domain EST (IMAGE:479159)
-2.4	2279	5428	Procollagen, type VI, alpha 1 (IMAGE:334132)
-2.4	992	2350	ESTs, highly similar to hypothetical 25.7-kD protein in MSH1-EPT1 intergenic region ( <i>Saccharomyces cerevisiae</i> ) (IMAGE:337654)
-2.4	329	787	Public domain EST (IMAGE:338162)

<sup>a</sup>Periostin, originally called OSF-2 (fasciclin I-like), is mainly detected in the periosteum and may play a role in the recruitment and attachment of osteoblast precursors (22)

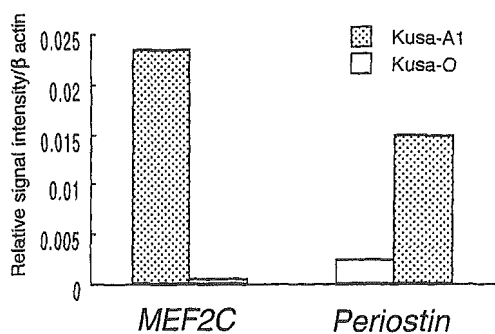


**Fig. 7.** *MEF2C* and *Periostin* expression in Kusa-A1 (gray bars) and Kusa-O (white bars). Reverse transcription-quantitative polymerase chain reaction (RT-qPCR) confirmed the data obtained by microarray (Table 2). In Kusa-A1, *MEF2C* was highly expressed, but *Periostin* expression was low. On the other hand, in Kusa-O, *MEF2C* expression was low, but *Periostin* expression was high

non-inducing condition, neither of these cell lines exhibited calcium deposits. These results imply that the recruitment of inorganic phosphate by ALP is a necessary but not sufficient condition to induce calcium deposition.

The differential expression of the osteogenic markers, *osteocalcin* and *osteopontin*, in Kusa-A1 and Kusa-O indicates their stage of osteogenesis. Osteocalcin, a kind of bone "gla" (gamma carboxy-glutamic acid) protein (BGP), is the major non-collagenous extracellular protein of bone tissue, and is thought to play an important role in bone mineral deposition with its gamma carboxy-glutamic acid residues [25]. *Osteopontin* is another osteogenic marker expressed in the middle stage of osteoblast differentiation in vitro. In this study, Kusa-A1 showed osteocalcin expression within 1 day after confluency in the inducing condition and 5 days after confluency in the non-inducing condition. But Kusa-O did not exhibit osteocalcin expression in either the inducing condition or the non-inducing condition. On the other hand, *osteopontin* expression was rather constant through the experimental time course in Kusa-O, but was high only in the inducing condition in Kusa-A1. To summarize these results, Kusa-A1 could be classified as a more mature stage of osteoblast than Kusa-O, a classification which is compatible with their osteogenesis/mineralization abilities in vivo and in vitro.

For Kusa-A1, some specific conditions have induced its differentiation into various types of cells. For example, Makino et al. [5] showed that Kusa-A1 differentiated into adipocytes or myotubes with 5-aza cytidine treatment. Moreover, the introduction of noggin, a suppressor of bone morphogenic protein (BMP) induced active neurons from Kusa-A1 [8]. These results indicate that Kusa should be considered as a kind of stem cell or progenitor cell, not as a simple osteoblastic cell line. We examined the expression of Notch signal-related genes that could be important for the regulation of various types of stem/progenitor cells. Notch signaling in stem cells models is often demonstrated as lateral inhibition or lateral specification [26,27]. These models well explain the "salt-and-pepper pattern" seen in the differentiation of stem cells [28], in which an active Notch

signal creates reciprocal patterns in neighboring cells. Our high-magnification view of calcified deposits in Kusa-A1 indicated this salt-and-pepper-like pattern, which may correspond to an activated Notch signal. In contrast, the obscure pattern of calcification in Kusa-O may indicate an inactive state of Notch signaling. In fact, our previous study demonstrated that a constitutively active form of Notch1 influenced the osteogenesis/mineralization ability of Kusa [29]. But Northern blot analysis showed that *HES1*, a downstream gene in the Notch signal pathway, changed its expression level only in Kusa-A1, in the non-inducing condition. The Notch signal has many different downstream factors, such as nuclear factor kappaB, p-300, Deltex, and mitogen-activated protein kinase (MAPK), other than the Epstein-Barr virus (EBV) latency C promoter binding factor 1 (CBF1)/hairly and enhancer of split 1 (HES1) pathway and employs them differentially. *HES1* may not be involved in the Notch signal pathway of Kusa.

Actually, the analysis of 588 cDNAs is not sufficient to use the term "global", but, with this small-number microarray, we detected that gross downregulation occurred in the inducing condition in both Kusa-A1 and Kusa-O. This indicates that "master gene expression" is not necessarily associated with osteogenesis/mineralization in Kusa, and conversely, the gross downregulation may carve out specific networks of signal pathways, resulting in the unidirectional differentiation of osteogenesis/mineralization. This hypothesis is a concept that is completely opposite to the "master gene theory", and further verification with other types of cell lines should be performed to test this hypothesis.

The high-throughput microarray (GEMarray), which was carried on Kusa-A1 and Kusa-O in the non-inducing condition, revealed a relatively high expression of *periostin* in Kusa-O cells. *Periostin* was identified from the screening of MC3T3-E1-specific genes, and sequence similarity analysis has revealed that it is homologous to fasciclin [30], a type of homophilic binding molecule [31,32]. *Periostin* is specifically expressed in the periosteum and the periodontal ligament [24]. The function of *periostin* remains to be elucidated, but recent reports indicate a relationship with cell attachment [33–36]. As compared with Kusa-A1, MC3T3-E1 in the non-inducing condition should be classified as showing a rather immature state of osteogenesis, and Kusa-O should also be included in this category. The high level of expression of *periostin* in MC3T3-E1 and Kusa-O may imply its role in the early stage of osteogenesis, although further investigation remains to be done to specify the molecular basis of this role.

In contrast to *periostin* expression in Kusa-A1, *MEF2C* showed enhanced expression. *MEF2C* is a basic/helix-loop-helix (bHLH) transcriptional factor and is known to be a late-stage regulator of myogenesis, under the control of *MyoD*, *Myf5*, and some other early myogenic genes [37–39]. However, we could not find upregulation of any other myogenic genes with the GEMarray microarray analysis. Recently, further roles and relationships of *MEF2C* have been found, such its action as an apoptotic factor in neurogenesis [40,41] and stem cell regulation, in the context of Notch

signaling, in both vertebrates and invertebrates [42]. As mentioned, it was difficult to find the direct involvement of *HES1* in the Notch pathway of Kusa, though activation of the Notch signal has been shown to suppress the differentiation of Kusa-A1 [29]. The Notch signal seems to employ some pathway(s) other than its classical one, and *MEF2C* could be a candidate. *CCN3* is a positive regulator of the Notch signal and its high expression in Kusa may be related to this kind of non-classical pathway of the Notch signal.

In conclusion, we investigated two sublines of Kusa from several different aspects and clarified their specific characteristics. Kusa seems to be a useful cell line, considering its high osteogenesis/mineralization activity; investigation of the molecular basis of this activity will give new insights for the technical development of osteogenic restitution.

**Acknowledgments** This work was supported by Grants-in-Aids from the Japanese Society for the Promotion of Science: no. 14370615 to N.K.; and nos. 15390552 and 12671763 to K.K.

## References

- Gershon D (2002) Microarray technology: an array of opportunities. *Nature* 416:885–891
- Pittenger MF, Mackay AM, Beck SC, Jaiswal RK, Douglas R, Mosca JD, Moorman MA, Simonetti DW, Craig S, Marshak DR (1999) Multilineage potential of adult human mesenchymal stem cells. *Science* 284:143–147
- Dexter TM, Testa NG (1976) Differentiation and proliferation of hemopoietic cells in culture. *Methods Cell Biol* 14:387–405
- Seale P, Rudnicki MA (2000) A new look at the origin, function, and “stem-cell” status of muscle satellite cells. *Dev Biol* 218:115–124
- Makino S, Fukuda K, Miyoshi S, Konishi F, Kodama H, Pan J, Sano M, Takahashi T, Hori S, Abe H, Hata J, Umezawa A, Ogawa S (1999) Cardiomyocytes can be generated from marrow stromal cells in vitro. *J Clin Invest* 103:697–705
- Umezawa A, Maruyama T, Segawa K, Shaddock RK, Waheed A, Hata J (1992) Multipotent marrow stromal cell line is able to induce hematopoiesis in vivo. *J Cell Physiol* 151:197–205
- Hall FL, Han B, Kundu RK, Yee A, Nimni ME, Gordon EM (2001) Phenotypic differentiation of TGF-beta1-responsive multipotent pre-mesenchymal prehematopoietic progenitor (P4 stem) cells from murine bone marrow. *J Hematother Stem Cell Res* 10:261–271
- Kohyama J, Abe H, Shimazaki T, Koizumi A, Nakashima K, Gojo S, Taga T, Okano H, Hata J, Umezawa A (2001) Brain from bone: efficient “meta-differentiation” of marrow stroma-derived mature osteoblasts to neurons with Noggin or a demethylating agent. *Differentiation* 68:235–244
- Mitaka T (2001) Hepatic stem cells: from bone marrow cells to hepatocytes. *Biochem Biophys Res Commun* 281:1–5
- Steidl U, Kronenwett R, Rohr UP, Fenk R, Kliszewski S, Maercker C, Neubert P, Aivado M, Koch J, Modlich O, Bojar H, Gattermann N, Haas R (2002) Gene expression profiling identifies significant differences between the molecular phenotypes of bone marrow-derived and circulating human CD34+ hematopoietic stem cells. *Blood* 99:2037–2044
- Sata M, Saiura A, Kunisato A, Tojo A, Okada S, Tokuhisa T, Hirai H, Makuuchi M, Hirata Y, Nagai R (2002) Hematopoietic stem cells differentiate into vascular cells that participate in the pathogenesis of atherosclerosis. *Nat Med* 8:403–409
- Lassar AB, Paterson BM, Weintraub H (1986) Transfection of a DNA locus that mediates the conversion of 10T1/2 fibroblasts to myoblasts. *Cell* 47:649–656
- Weintraub H, Davis R, Tapscott S, Thayer M, Krause M, Benezra R, Blackwell TK, Turner D, Rupp R, Hollenberg S, Zhuang Y, Lassar A (1991) The myoD gene family: nodal point during specification of the muscle cell lineage. *Science* 251:761–766
- Tontonoz P, Hu E, Spiegelman BM (1994) Stimulation of adipogenesis in fibroblasts by PPAR gamma 2, a lipid-activated transcription factor. *Cell* 79:1147–1156
- Komori T, Yagi H, Nomura S, Yamaguchi A, Sasaki K, Deguchi K, Shimizu Y, Bronson RT, Gao YH, Inada M, Sato M, Okamoto R, Kitamura Y, Yoshiki S, Kishimoto T (1997) Targeted disruption of *Cbfa1* results in a complete lack of bone formation owing to maturational arrest of osteoblasts. *Cell* 89:755–764
- Nakashima K, Zhou X, Kunkel G, Zhang Z, Deng JM, Behringer RR, de Crombrughe B (2002) The novel zinc finger-containing transcription factor osterix is required for osteoblast differentiation and bone formation. *Cell* 108:17–29
- Rodan GA, Noda M (1991) Gene expression in osteoblastic cells. *Crit Rev Eukaryot Gene Expr* 1:85–98
- Yasui N, Ochi T, Takaoka K, Ono K, Nakata Y (1980) Osteogenesis by factor(s) isolated from mouse osteosarcoma cells in combination with collagen. *Biken J* 23:83–87
- Chen JJ, Wu R, Yang PC, Huang JY, Sher YP, Han MH, Kao WC, Lee PJ, Chiu TF, Chang F, Chu YW, Wu CW, Peck K (1998) Profiling expression patterns and isolating differentially expressed genes by cDNA microarray system with colorimetry detection. *Genomics* 51:313–324
- Ecarot-Charrier B, Glorieux FH, van der Rest M, Pereira G (1983) Osteoblasts isolated from mouse calvaria initiate matrix mineralization in culture. *J Cell Biol* 96:639–643
- Schoeters GE, de Saint-Georges L, Van den Heuvel R, Vanderborcht O (1988) Mineralization of adult mouse bone marrow in vitro. *Cell Tissue Kinet* 21:363–374
- Celeste AJ, Rosen V, Buecker JL, Kriz R, Wang EA, Wozney JM (1986) Isolation of the human gene for bone gla protein utilizing mouse and rat cDNA clones. *Embo J* 5:1885–1890
- Nomura S, Wills AJ, Edwards DR, Heath JK, Hogan BL (1988) Developmental expression of 2ar (osteopontin) and SPARC (osteonectin) RNA as revealed by in situ hybridization. *J Cell Biol* 106:441–450
- Horiuchi K, Amizuka N, Takeshita S, Takamatsu H, Katsuura M, Ozawa H, Toyama Y, Bonewald LF, Kudo A (1999) Identification and characterization of a novel protein, periostin, with restricted expression to periosteum and periodontal ligament and increased expression by transforming growth factor beta. *J Bone Miner Res* 14:1239–1249
- Boskey AL, Gadaleta S, Gundberg C, Doty SB, Ducy P, Karsenty G (1998) Fourier transform infrared microspectroscopic analysis of bones of osteocalcin-deficient mice provides insight into the function of osteocalcin. *Bone* 23:187–196
- Sternberg PW (1988) Lateral inhibition during vulval induction in *Caenorhabditis elegans*. *Nature* 335:551–554
- Freitas C, Rodrigues S, Charrier JB, Teillet MA, Palmeirim I (2001) Evidence for medial/lateral specification and positional information within the presomitic mesoderm. *Development* 128:5139–5147
- Marnellos G, Deblandre GA, Mjolsness E, Kintner C (2000) Delta-Notch lateral inhibitory patterning in the emergence of ciliated cells in *Xenopus*: experimental observations and a gene network model. *Pac Symp Biocomput* 5:329–340
- Shindo K, Kawashima N, Sakamoto K, Yamaguchi A, Umezawa A, Takagi M, Katsube K, Suda H (2003) Osteogenic differentiation of mesenchymal progenitor cells, Kusa is suppressed by Notch signaling. *Exp Cell Res* 290:370–380
- Takeshita S, Kikuno R, Tezuka K, Amann E (1993) Osteoblast-specific factor 2: cloning of a putative bone adhesion protein with homology with the insect protein fasciclin I. *Biochem J* 294 (Pt 1):271–278
- Elkins T, Hortsch M, Bieber AJ, Snow PM, Goodman CS (1990) *Drosophila* fasciclin I is a novel homophilic adhesion molecule that along with fasciclin III can mediate cell sorting. *J Cell Biol* 110:1825–1832
- Elkins T, Zinn K, McAllister L, Hoffmann FM, Goodman CS (1990) Genetic analysis of a *Drosophila* neural cell adhesion molecule: interaction of fasciclin I and Abelson tyrosine kinase mutations. *Cell* 60:565–575
- Shao R, Bao S, Bai X, Blanchette C, Anderson RM, Dang T, Gishizky ML, Marks JR, Wang XF (2004) Acquired

- expression of periostin by human breast cancers promotes tumor angiogenesis through up-regulation of vascular endothelial growth factor receptor 2 expression. *Mol Cell Biol* 24:3992–4003
34. Nakazawa T, Nakajima A, Seki N, Okawa A, Kato M, Moriya H, Amizuka N, Einhorn TA, Yamazaki M (2004) Gene expression of periostin in the early stage of fracture healing detected by cDNA microarray analysis. *J Orthop Res* 22:520–525
  35. Kudo H, Amizuka N, Araki K, Inohaya K, Kudo A (2004) Zebrafish periostin is required for the adhesion of muscle fiber bundles to the myoseptum and for the differentiation of muscle fibers. *Dev Biol* 267:473–487
  36. Bao S, Ouyang G, Bai X, Huang Z, Ma C, Liu M, Shao R, Anderson RM, Rich JN, Wang XF (2004) Periostin potently promotes metastatic growth of colon cancer by augmenting cell survival via the Akt/PKB pathway. *Cancer Cell* 5:329–339
  37. Takebayashi-Suzuki K, Pauliks LB, Eltsefon Y, Mikawa T (2001) Purkinje fibers of the avian heart express a myogenic transcription factor program distinct from cardiac and skeletal muscle. *Dev Biol* 234:390–401
  38. Sartorelli V, Huang J, Hamamori Y, Kedes L (1997) Molecular mechanisms of myogenic coactivation by p300: direct interaction with the activation domain of MyoD and with the MADS box of MEF2C. *Mol Cell Biol* 17:1010–1026
  39. Edmondson DG, Lyons GE, Martin JF, Olson EN (1994) Mef2 gene expression marks the cardiac and skeletal muscle lineages during mouse embryogenesis. *Development* 120:1251–1263
  40. Okamoto S, Krainc D, Sherman K, Lipton SA (2000) Antiapoptotic role of the p38 mitogen-activated protein kinase-myocyte enhancer factor 2 transcription factor pathway during neuronal differentiation. *Proc Natl Acad Sci U S A* 97:7561–7566
  41. Okamoto S, Li Z, Ju C, Scholzke MN, Mathews E, Cui J, Salvesen GS, Bossy-Wetzel E, Lipton SA (2002) Dominant-interfering forms of MEF2 generated by caspase cleavage contribute to NMDA-induced neuronal apoptosis. *Proc Natl Acad Sci U S A* 99:3974–3979
  42. Wilson-Rawls J, Molkenstein JD, Black BL, Olson EN (1999) Activated notch inhibits myogenic activity of the MADS-Box transcription factor myocyte enhancer factor 2C. *Mol Cell Biol* 19:2853–2862

# Immortalization of Human Fetal Cells: The Life Span of Umbilical Cord Blood-derived Cells Can Be Prolonged without Manipulating p16<sup>INK4a</sup>/RB Braking Pathway<sup>□</sup>

Masanori Terai,\*<sup>†</sup> Taro Uyama,\* Tadashi Sugiki,\* Xiao-Kang Li,<sup>‡</sup>  
Akihiro Umezawa,\*<sup>§</sup> and Tohru Kiyono<sup>†</sup>

Departments of \*Reproductive Biology and Pathology and <sup>†</sup>Innovative Surgery, National Research Institute for Child Health and Development, Tokyo 157-8535, Japan; <sup>‡</sup>Virology Division, National Cancer Center Research Institute, Tokyo, Japan; and <sup>§</sup>Department of Pathology, Keio University School of Medicine, Tokyo 160-8582, Japan

Submitted July 31, 2004; Accepted December 20, 2004  
Monitoring Editor: Lawrence Goldstein

Human umbilical cord blood-derived mesenchymal stem cells (UCBMSCs) are expected to serve as an excellent alternative to bone marrow-derived human mesenchymal stem cells. However, it is difficult to study them because of their limited life span. To overcome this problem, we attempted to produce a strain of UCBMSCs with a long life span and to investigate whether the strain could maintain phenotypes in vitro. UCBMSCs were infected with retrovirus carrying the human telomerase reverse transcriptase (hTERT) to prolong their life span. The UCBMSCs underwent 30 population doublings (PDs) and stopped dividing at PD 37. The UCBMSCs newly established with hTERT (UCBTERTs) proliferated for >120 PDs. The p16<sup>INK4a</sup>/RB braking pathway leading to senescence can be inhibited by introduction of Bmi-1, a polycomb-group gene, and human papillomavirus type 16 E7, but the extension of the life span of the UCBMSCs with hTERT did not require inhibition of the p16<sup>INK4a</sup>/RB pathway. The characteristics of the UCBTERTs remained unchanged during the prolongation of life span. UCBTERTs provide a powerful model for further study of cellular senescence and for future application to cell-based therapy by using umbilical cord blood cells.

## INTRODUCTION

Human mesenchymal stem cells (hMSCs) can be a useful source of cells for transplantation for several reasons: they have the ability to proliferate and differentiate into mesodermal tissues, and they entail no ethical or immunological problems (Caplan, 1991; Prockop, 1997; Caplan and Bruder, 2001). hMSCs have been studied extensively over the past 3 decades, and numerous independent research groups have successfully isolated hMSCs from a variety of sources, most commonly, from the bone marrow (Owen, 1988; Umezawa *et al.*, 1992; Jaiswal *et al.*, 1997; Makino *et al.*, 1999; Pittenger *et al.*, 1999; Sekiya *et al.*, 2004). Umbilical cord blood (UCB) contains circulating stem/progenitor cells, and the cells contained in UCB are known to be distinct from those contained in bone marrow and adult peripheral blood (Mayani and Lansdorp, 1998). Isolation, characterization, and differentiation of clonally expanded hMSCs derived from UCB (UCBMSCs) have been reported (Goodwin *et al.*, 2001; Lee *et al.*, 2004), and UCBMSCs have been found to have multipotency, and the immunophenotype of the clonally expanded cells is consistent with that reported for bone marrow mes-

enchymal stem cells. Even now, most UCB is regarded as medical waste in the delivery rooms. Aspirating bone marrow from patients is, however, an invasive procedure, and the proliferation and differentiation capacity of hMSCs decreases with the donor age (D'Ippolito *et al.*, 1999). Therefore, the applications of UCB should be further expanded.

UCBMSCs will be useful sources for cell transplantation, however, it is difficult to study and apply them because of their limited life span. One of the reasons for this is that normal human cells undergo a limited number of cell division in culture and then enter a nondividing state called "senescence" (Hayflick, 1976; Campisi, 1997). Human cells reach senescence or cease to divide after a limited number of cell replications, and the average number of hMSC population doublings (PDs) has been found to be ~40 (Takeda *et al.*, 2004), implying that it would be difficult to obtain enough cells to restore the function of a failing human organ. Large numbers of cells must be injected into damaged tissues to restore function in humans, and cells sometimes need to be injected throughout entire organs.

To resolve these problems, the life span of hMSCs from bone marrow can be extended by retroviral transduction of human telomerase reverse transcriptase (hTERT) (Blackburn, 2000a,b, 2001) and human papillomavirus type 16 (HPV16) E6 and/or E7 (Sekiguchi *et al.*, 1999; Burk *et al.*, 2003; Takeda *et al.*, 2004). Both p16<sup>INK4a</sup>/RB inactivation with E7 and telomerase activation with E6 are required to extend the life span of human mammary epithelial cells (Kiyono *et al.*, 1998). E6 also accelerates degradation of p53, which induces the cdk inhibitor p21 (Sekiguchi and Hunter, 1998). This system in which p16<sup>INK4a</sup>/RB is inhibited and

This article was published online ahead of print in *MBC in Press* (<http://www.molbiolcell.org/cgi/doi/10.1091/mbc.E04-07-0652>) on January 12, 2005.

<sup>□</sup> The online version of this article contains supplemental material at *MBC Online* (<http://www.molbiolcell.org>).

Address correspondence to: Akihiro Umezawa (umezawa@1985.jukuin.keio.ac.jp).

telomerase is activated is highly efficient in extending the life span of hMSCs (Okamoto *et al.*, 2002).

In the present study, we investigated the growth regulatory mechanism of UCBMSCs and attempted to establish UCBMSCs with hTERT (UCBTERTs) to overcome their limited life span. Introduction of hTERT alone was sufficient to extend the life span of UCBMSCs in vitro, and this technique for prolonging the life span of UCBMSCs will be a useful tool. UCBTERTs with the extended life span provide a powerful model for further study of cellular senescence and application to transplantation therapy in the future.

## MATERIALS AND METHODS

### Isolation and Cell Culture of UCBMSCs

UCB was collected on delivery with informed consent. UCB mononuclear cells were obtained as per the manufacturer's instructions, followed by Ficoll-Paque (Amersham Biosciences, Piscataway, NJ) density gradient centrifugation (1.077 g/cm<sup>3</sup>), and plated in tissue culture dishes (BD Biosciences, San Jose, CA) in DMEM medium (Sigma-Aldrich, St. Louis, MO) and 10% fetal bovine serum (FBS) (Vitromex, Geilenkirchen, Germany). All cultures were maintained at 37°C in a humidified atmosphere containing 95% air and 5% CO<sub>2</sub>. A few colonies were found in the culture dish 1 mo after the collected cells were cultured in DMEM with 10% FBS. One colony was trypsinized using a colony cylinder and then diluted and plated on 12-well plates (BD Biosciences) in mesenchymal stem cell growth medium (MSCGM, PT-3001; Cambrex Bio Science Walkersville, Walkersville, MD) at a final density of  $\sim 4 \times 10^5$  cells/well in a 12-well plate. MSCGM was used in all culture procedures after harvesting the colony. The cells were passaged at a density of  $\sim 1 \times 10^5$  cells/100-mm dish (1:4), and the original cells were regarded as being PD 0 (day 0). When the cultures reached subconfluence, the cells were harvested with 0.25% trypsin and 1 mM EDTA and replated with one-half of the harvested cells. Cells were allowed to adhere overnight, and nonadherent cells were washed out with medium changes. Medium changes were carried out twice weekly thereafter. The cells were cultured for further experiments under the approval (approval nos. 7 and 55) of the Ethics Committee of National Research Institute for Child Health and Development, Tokyo.

### Infection with Recombinant Retroviruses

The cells were prepared for infection with recombinant retroviruses expressing the E6, E7, and hTERT, as described previously (Takeda *et al.*, 2004). Stably transduced cells with an expanded life span were designated UCBE6E7-20 and UCBTERT-21 cells.

### Senescence-associated- $\beta$ -gal (SA- $\beta$ -gal) Staining

The SA- $\beta$ -gal assay was performed as described previously (Dimri *et al.*, 1995). Cells were washed in phosphate-buffered saline (PBS), fixed for 3–5 min at room temperature in 2% formaldehyde/0.2% glutaraldehyde (or 3% formaldehyde), washed, and incubated at 37°C with fresh SA- $\beta$ -gal stain solution: 1 mg of 5-bromo-4-chloro-3-indolyl  $\beta$ -D-galactosidase per milliliter (stock is 20 mg of dimethylformamide/ml), 40 mM citric acid/sodium phosphate, pH 6.0, 5 mM potassium ferrocyanide, 5 mM potassium ferricyanide, 150 mM NaCl, and 2 mM MgCl<sub>2</sub>. Staining was evident in 2–4 h and maximal in 12–16 h.

### Cell Transplantation

Freshly collected confluent cells ( $10^6$  cells) were subcutaneously and intramuscularly injected into BALB/c nu/nu mice (Sankyo Laboratory, Hamamatsu, Japan). Animals were monitored for malignant transformation of the injected cells for 3 mo after inoculation and then killed by cervical location.

### Flow Cytometric Analysis

Cells were stained for 30 min at 4°C with primary antibodies and immunofluorescent secondary antibodies. The cells were then analyzed on a FACScan (BD Biosciences), and the data were analyzed with the CELLQUEST software (BD Biosciences). Antibodies against human CD13, CD14, CD29, CD31, CD34, CD44, CD45, CD50, CD55, CD59, CD90, CD117, and CD133 were purchased from Beckman Coulter (Fullerton, CA), Immunotech (Marseille, France), Cytotech (Hellebaek, Denmark), and BD Biosciences PharMingen (San Diego, CA).

### Western Blot Analysis

Cells were seeded at a density of  $3 \times 10^5$  cells/100-mm culture dish and harvested at subconfluence. Cell lysates were prepared by sonication by using ultrasonic homogenizer VP-55 in WE16th lysis buffer (Gewin *et al.*, 2004). Equal amounts of protein (20  $\mu$ g) were loaded on SDS-polyacrylamide gels

and blotted on Immobilon-P membranes (Millipore, Bedford, MA) by using a semidry transfer system (Atto, Tokyo, Japan). The primary antibodies used were as follows: G3-245 for retinoblastoma (RB) protein and G175-405 for p16<sup>INK4a</sup> (BD Biosciences PharMingen), DO-1 for p53 (Oncogene Science, Cambridge, MA), F-5 for p21 and I-19 for actin (Santa Cruz Biotechnology, Santa Cruz, CA), affinity-purified anti-phospho-ataxia telangiectasia mutated kinase (p-ATM) (Ser1981) (600-401-400; Rockland, Gilbertsville, PA), and phospho-p53 (p-p53) (Ser15) antibody (9284; Cell Signaling Technology, Beverly, MA). Blots were probed with horseradish peroxidase-conjugated goat anti-mouse IgG (Jackson ImmunoResearch Laboratories, West Grove, PA), anti-rabbit IgG (New England Biolabs, Beverly, MA), or donkey anti-goat IgG (Santa Cruz Biotechnology), and visualized using an enhanced chemiluminescence detection kit (Roche Diagnostics, Indianapolis, IN).

### Telomere Length Assay

Total genomic DNA was isolated from cultured cells by proteinase K digestion. The lengths of telomere in each sample were determined by Southern blot analysis as described previously (Vaziri *et al.*, 1994). Briefly, 1  $\mu$ g of genomic DNA extracted from each sample was digested with both *Hinf*I and *Rsa*I and electrophoresed in 0.8% agarose gels for 16 h, transferred onto a Hybond N membrane (Amersham Biosciences), and hybridized with digoxigenin (DIG)-labeled (TTAGGG)<sub>3</sub> probe. The membrane was incubated with anti-DIG alkaline phosphatase (ALP) antibody, and detection was performed with chemiluminescence solution.

### Telomerase Activity

Telomerase activity in each sample was detected by the telomeric repeat amplification protocol (TRAP) assay by using the TRAPeze kit (Intergen, Purchase, NY) according to the manufacturer's instruction.

### Karyotype Analysis

Fixation and chromosome preparation were performed according to the standard procedure described previously (Sasaki, 1975). For each sample, >50 cells were scored for their chromosome number.

### Differentiation-Induction Experiments

The multidirectional differentiation potential of each cell line was assessed by the differentiation-induction protocols described below.

### Histochemical Staining

After 21 d of culture, cells were rinsed twice with PBS and then fixed with 10% buffered formalin for 10 min at room temperature. The fixed cells were stained with 0.3% Oil-Red-O (Nakarai Tesque, Kyoto, Japan) for the adipogenic differentiation assay and with 5% silver nitrate (Nakarai Tesque) for von Kossa staining in the osteogenic differentiation assay (Tsuchiya *et al.*, 2004).

### Osteogenic Differentiation

Cells were seeded at a density of  $5 \times 10^4$  cells/cm<sup>2</sup> in tissue culture dishes and cultured with MSCGM containing 100 nM dexamethasone, 50  $\mu$ M ascorbic acid 2-phosphate, and  $\beta$ -glycerophosphate. The cultures were maintained for 4 wk, and the cultured medium was replaced every 3 d.

### Adipogenic Differentiation

Cells were seeded at a density of  $3 \times 10^4$  cells/cm<sup>2</sup> in tissue culture dishes. When the cells were confluent, the adipogenic differentiation was initiated by three cycles of induction/maintenance culture. Each cycle consists of 3 d of culture in the induction medium (DMEM with 10% FBS, 1  $\mu$ M dexamethasone, 0.2 mM indomethacin, 10  $\mu$ g/ml insulin, and 0.5 mM 3-isobutyl-1-methylxanthine) followed by 2 d of culture in the maintenance medium (DMEM with 10% FBS and 10  $\mu$ g/ml insulin).

## RESULTS

### Establishment of UCB-derived Cells with an Extended Life Span

UCBMSCs regarded as being PD 0, or day 0, were fibroblast-like in morphology, indistinguishable in appearance from the marrow-derived MSCs, and relatively larger in size than rapidly self-renewing stem cells (Prockop *et al.*, 2001) and multipotent adult progenitor stem cells (Jiang *et al.*, 2002) (Figure 1A). The cells from PD 9 to PD 31 rapidly proliferated in culture, and propagated continuously (Figure 1, B and C). No SA- $\beta$ -gal activity was detected histoenzymologically in the UCBMSCs in the growth phase on day 59. The UCBMSCs stopped replicating, became broad and flat, and exhibited SA- $\beta$ -gal activity as indicated by blue staining of



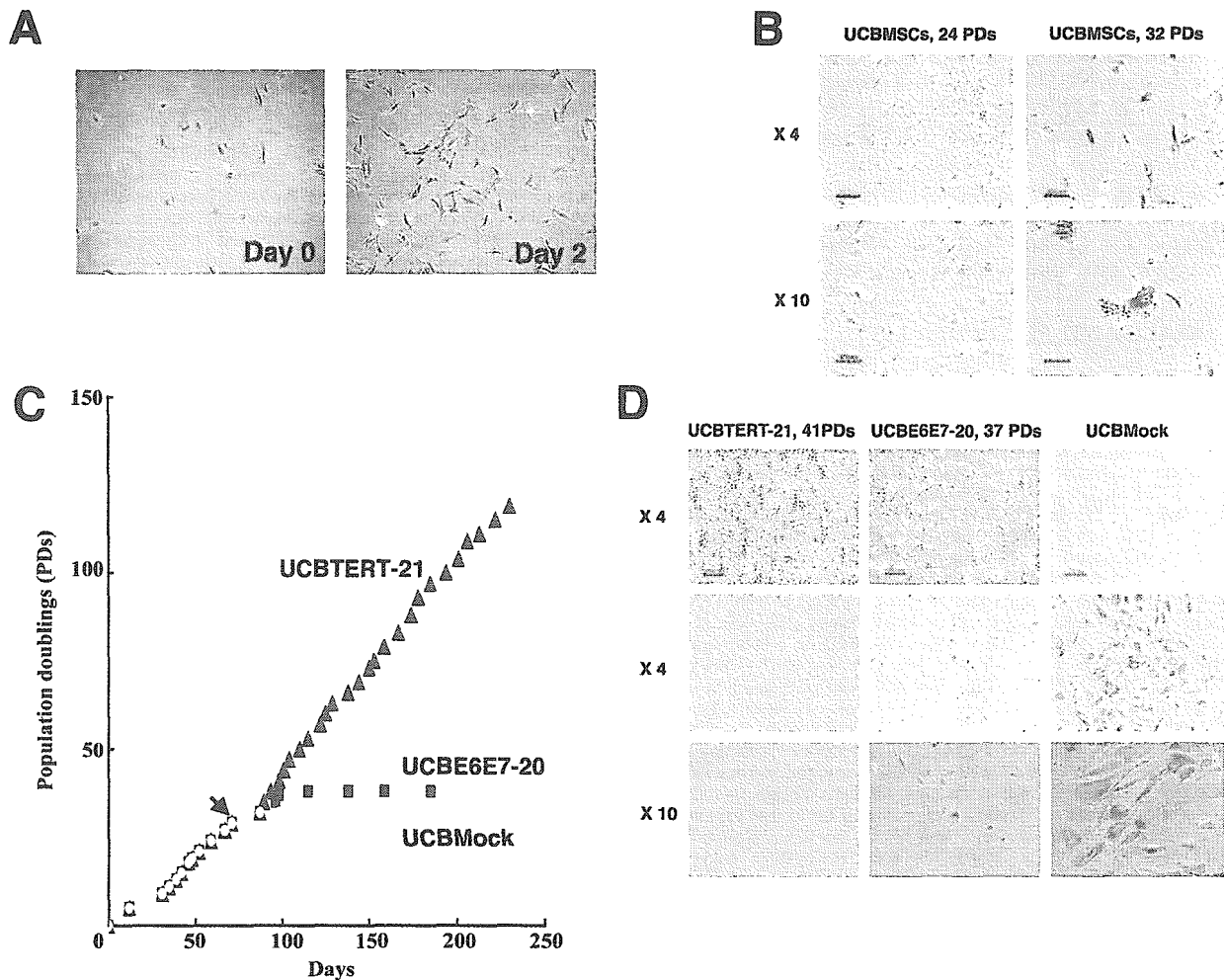


**Figure 1.** In vitro growth and SA- $\beta$ -gal activity of UCBMSCs, UCBE6E7-20 cells, and UCBTERT-21 cells. (A) Morphology of human UCBMSCs (left, day 0; right, day 2; original magnification, 10 $\times$ ). (B) Morphological changes and SA- $\beta$ -gal activity of UCBMSCs. UCBMSCs were a broad and flat, ceased to proliferate, and exhibited high SA- $\beta$ -gal activity as indicated by their cytoplasm staining blue at PD 32 (14 passages at day 98), suggesting senescence. No SA- $\beta$ -gal activity was detected in the UCBMSCs in the growth phase at PD 24 (10 passages at day 59 in left column). Bar, 250  $\mu$ m in the upper column and 100  $\mu$ m in the lower column. (C) Population doublings of UCBMock cells (yellow circles), UCBE6E7-20 cells (red squares), and UCBTERT-21 cells (blue triangles) are shown. UCBMSCs were infected with recombinant retroviruses carrying E6 and E7 or hTERT or were treated with polybrene alone at PD 29 (indicated as an arrow). UCBTERT-21 cells proliferated for >120 PDs and for >250 d and exhibited persistent growth. UCBE6E7-20 cells exhibited a prolonged cell life span in culture, reached 38 PDs, and then entered crisis. UCBMock cells stopped growing and entered senescence at 32 PDs. (D) Morphological changes (top column) and SA- $\beta$ -gal activity (middle and bottom column) of UCBMock cells, UCBE6E7-20 cells, and UCBTERT-21 cells. No staining was detected in UCBTERT-21 cells at PD 41 (left column, 16 passages at day 98) with the SA- $\beta$ -gal stain (middle and bottom columns). A few UCBE6E7 cells were positive with SA- $\beta$ -gal stain at PD 37 (middle column, 15 passages at day 98). UCBMock cells were broad and flat at PD 32 (right column, 14 passage at day 98), indicating senescence.

their cytoplasm at PD 32 or day 98, indicating that they had entered senescence (Figure 1, B and C). The morphological changes and SA- $\beta$ -gal activity of UCBMSCs are PD dependent. To extend the cells' life span and obtain a large number of cells, two different types of cells were obtained by transferring a combination of HPV16 E6 and E7 or hTERT at 29 PDs or 12 passages (Figure 1C, indicated as an arrow). UCBMSCs transduced with a combination of E6 and E7 were designated UCBE6E7-20 cells, and UCBMSCs transduced with hTERT were named UCBTERT-21 cells. UCBTERT-21 cells successfully proliferated >120 PDs, and continued to grow. The cells were found to have an extended life span (Figure 1C, UCBTERT-21 cells, blue triangles). The UCBE6E7-20 cells, which had been transduced with E6 and E7, had a prolonged cell life span in culture, and underwent global cell death at 38 PDs,

when the cells entered a "crisis" period. This implies that the E6 and E7 are capable of prolonging cell life span but that their effect is limited (Figure 1C, UCBE6E7-20 cells, pink squares). Mock infection (polybrene treatment alone) did not extend cell life span, and the cells reached senescence or cessation of growth at PD 32 (Figure 1C, UCBMock, yellow circles). SA- $\beta$ -gal staining was performed to determine the proportions of cells that had entered senescence, and positive staining was observed in 0% of the UCBTERT-21 cells at PD 41, 2% of the UCBE6E7-20 cells at PD 37, and 100% of the UCBMock cells at PD 32 (Figure 1D). The low percentage of SA- $\beta$ -gal-positive UCBE6E7-20 cells at PD 37 or day 98 is probably attributable to global cell death by crisis (Figure 1D, middle column). UCBMock cells exhibited a typical senescence-associated morphology, i.e., they were broad and flat and exhibited strong SA- $\beta$ -

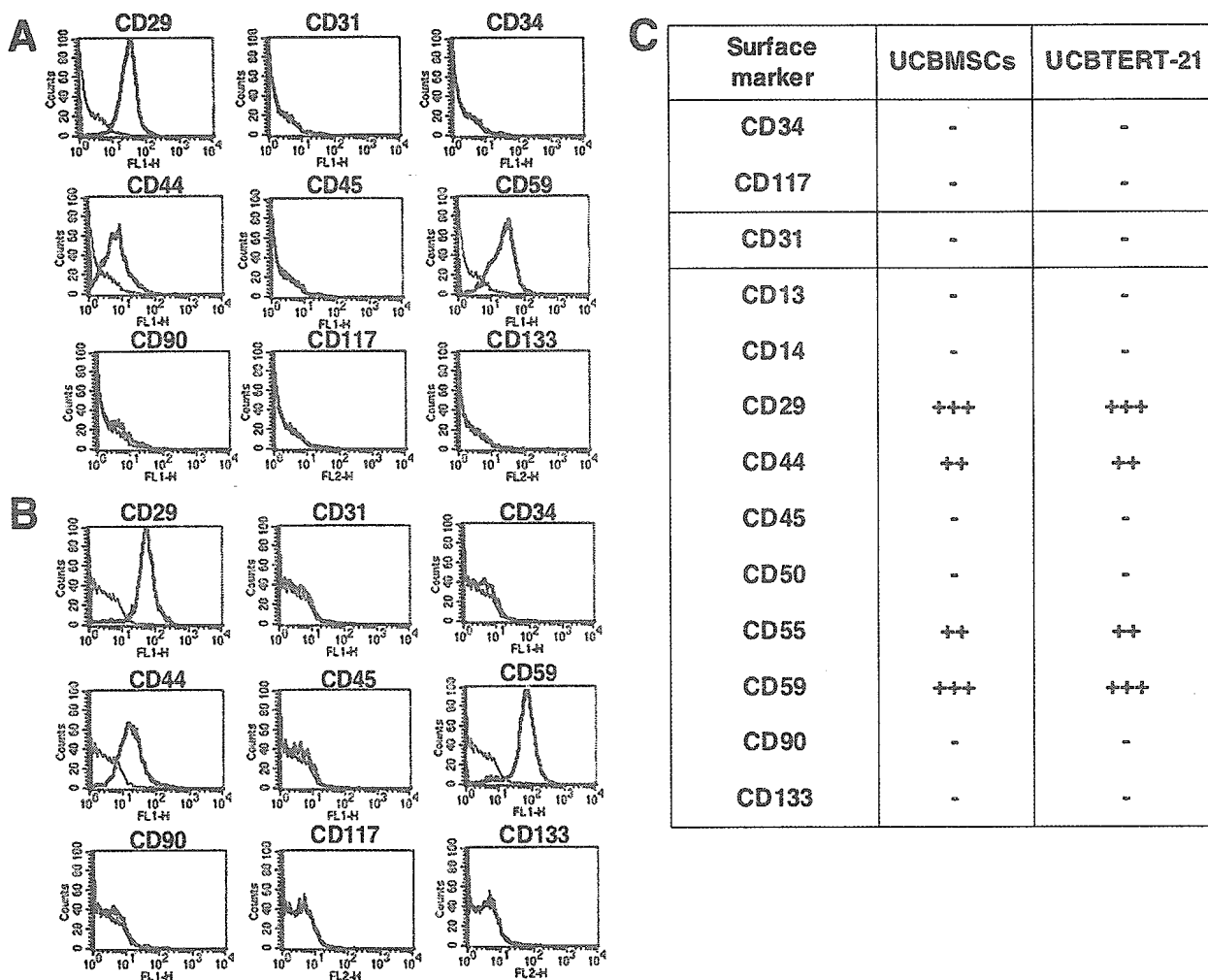


**Figure 2.** Flow cytometric analysis of cell surface markers of UCBMSCs and UCBTERT-21 cells. UCBMSCs (A) displayed the same pattern of surface markers as UCBTERT-21 cells (B). No difference in cell surface markers was found between UCBMSCs and UCBTERT-21 cells as summarized in the table (C). Both were positive for CD29 (integrin  $\beta$ 1), CD44 (Pgp-1/ly-24), and CD59, and negative for CD31 (PECAM-1), CD34, CD45 (leukocyte common antigen), CD90 (Thy-1), CD117 (c-kit), and CD133.

gal activity enzyme cytochemically at PD 32 (Figure 1D, right column).

The cells did not undergo malignant transformation. They stopped dividing after reaching confluence, and they did not form any foci after confluence in vitro. Nor did the cells grafted into the subcutaneous and muscle tissue of nude mice ( $n = 6$ ) produce tumors, at least during the monitoring period ( $>100$  d). Injected UCBTERT-21 cells survived but did not proliferate at the injection sites.

#### Unchanged Surface Markers of UCBMSCs after Prolongation of Their Life Span

Expression of UCBMSCs and UCBTERT-21 cell surface markers was evaluated by flow cytometric analysis (Figure 2). The results showed that both cells were positive for CD29 (integrin  $\beta$ 1), CD44 (Pgp-1/ly-24), CD55, and CD59, and negative for CD13, CD14 (a marker for macrophages and dendritic cells), CD31 (platelet-endothelial cell adhesion molecule-1, PECAM-1), CD34, CD45 (leukocyte common antigen), CD50 (intercellular adhesion molecule-1, ICAM-1), CD90 (Thy-1), CD117 (c-kit), and CD133. Primary UCBMSCs displayed the same pattern of surface markers as UCB-

TERT-21 cells, implying that the surface marker expression was unaffected by the exogenously expressed hTERT.

#### Absence of p16<sup>INK4a</sup> in Parental UCBMSCs

Expression of p16<sup>INK4a</sup>/RB premature senescence-associated proteins (Figure 3A) and telomere/p53 replicative senescence-associated proteins (Figure 3B) was analyzed in UCBMSCs, UCBTERT-21, and UCBE6E7-20 cells. p16<sup>INK4a</sup> was not detected in the UCBMSC lanes until the senescence stage; p16<sup>INK4a</sup> was not detected until PD 53 and started to be expressed in UCBTERT-21 cells at a low level at PD 69, and p16<sup>INK4a</sup> was detected in UCBE6E7-20 cells at PD 37, immediately before the crisis stage. The protein levels of p53 and p21 in UCBMSCs became up-regulated as the number of PDs increased, but the protein levels of p53 and p21 became down-regulated in UCBE6E7-20 cells, implying that exogenously introduced E6 targets p53 for proteolytic degradation. ATM in UCBE6E7-20 cells was phosphorylated, probably because of DNA damage or telomere length shortening (Figure 3B, lane 8). p53, phosphorylated p53, and p21 were induced by H<sub>2</sub>O<sub>2</sub>, a physiological stressor, in UCBTERT-21 cells (Figure 3B, lane 9). The hypophosphorylated forms of

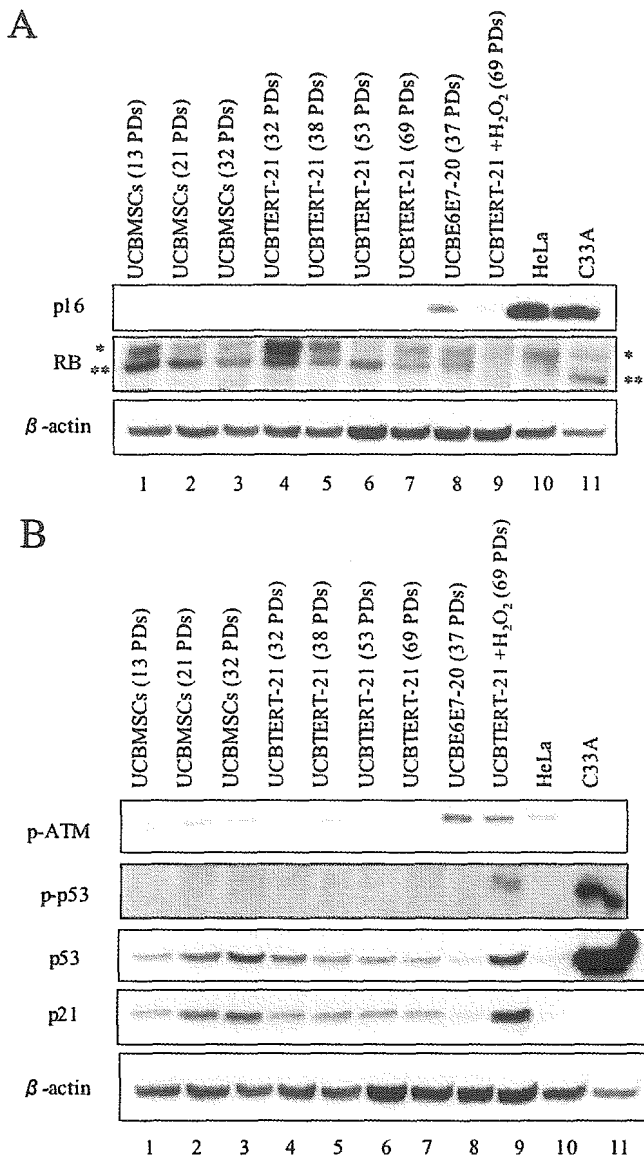


**Figure 3.** Time-course analysis of cell cycle-associated protein levels in UCBMSCs, UCBE6E7-20 cells, and UCBTERT-21 cells. UCBMSCs, UCBE6E7-20 cells, and UCBTERT-21 cells were analyzed by Western blotting for cell cycle-associated p16<sup>INK4a</sup>, RB, p-ATM (Ser1981), phospho-p53 (p-p53) (Ser15), p53, p21 and  $\beta$ -actin protein levels. (A) "p16<sup>INK4a</sup>-RB" senescence (premature senescence) pathway-associated protein levels, i.e., p16<sup>INK4a</sup> and RB. The hyperphosphorylated and hypophosphorylated forms of RB were indicated as a single asterisk and double asterisks, respectively. (B) Telomere shorten-p53' senescence (replicative senescence) pathway-associated protein levels, i.e., p-ATM, p-p53, p53, and p21. Cells were cultured for the PDs indicated and assayed. Expression of  $\beta$ -actin protein was monitored as a loading control.

RB became dominant and the hyperphosphorylated forms decreased with passage of UCBMSCs (Figure 3A, lanes 1–3), correlating to the increase in p53 and p21 (Figure 3B, lanes 1–3) and to the decrease in cell growth. Transduction of hTERT transiently and markedly increased the hyperphosphorylated form (Figure 3A, lane 4), corresponding to the sudden recovery in proliferation and to a shorter doubling time. Finally, both hyper- and hypophosphorylated forms of RB remained at steady-state levels (Figure 3A, lanes 5–7),

although the hypophosphorylated form seemed dominant at PD 53 (Figure 3A, lane 6), perhaps due to the higher cell density at collection of cell lysate. The protein level of RB was down-regulated in E7-overexpressing UCBE6E7-20 cells (Figure 3A, lane 8), probably as a result of enhanced proteolysis by E7.

#### Increase in Telomerase Activity and Maintenance of Telomere Length in Cells Transduced with the hTERT

Telomerase activity is revealed by the characteristic six base pair ladder of bands detected by TRAP assay (Figure 4A). No telomerase activity was detected in UCBMSCs at any PDs tested, UCBE6E7-20 cells, UCBMSCs infected with the vector-alone or CHAPS buffer, or mock infected. By contrast, the cells transduced with the hTERT exhibited significant levels of telomerase activity, comparable to HeLa cells as a positive control and to TSR8, which is a synthetic template of eight telomeric repeats used as a polymerase chain reaction (PCR)-positive control.

Average telomere length was longer in the UCBTERT-21 cells than in UCBMSCs. Telomere length in UCBMSCs decreased with the number of PDs, whereas it remained the same in UCBTERT-21 cells, regardless of the number of PDs. The telomere length of UCBE6E7-20 cells was shorter than that of the parental UCBMSCs at senescence.

#### Normal Diploid Karyotypes with XY Sex Chromosomes in UCBMSCs and UCBTERT-21 Cells

Karyotypic analyses of UCBMSCs were performed at PD 5 (2 passages) and of UCBTERT-21 cells at PD 32 (14 passages). UCBMSCs and UCBTERT-21 cells were found to be diploid and not to exhibit any significant chromosomal abnormalities (Figure 5, A and B). The chromosome number of both UCBMSCs at PD 5 and UCBTERT-21 cells at PD 35 was 46, except for one UCBTERT-21 cell, which contained 47 chromosomes (Figure 5C). No UCBTERT-21 cells containing abnormal numbers of chromosome were found on further analysis. The sex chromosomes were found to be XY, indicating that the cells were of fetal origin.

#### Osteogenic and Adipogenic Differentiation Potentials of UCBMSCs and UCBTERT-21 Cells

The multipotency of UCBMSCs and UCBTERT-21 cells was assessed by conventional protocols. The osteogenic differentiation potential of UCBMSCs and UCBTERT-21 cells was assessed based on their morphology and von Kossa staining after 3 wk of induction (Figure 6). Multiple small Oil-Red-O-positive fat droplets had accumulated in UCBMSCs and UCBTERT-21 cells after 3 and 2 wk, respectively, of adipogenic induction. Adipocyte differentiation was estimated by counting 2000 cells per dish. The results of triplicate experiments showed that 5.0 and 5.4% of the UCBMSC and UCBTERT-21 cells became positive for fat droplets with Oil-Red stain as a result of adipogenic induction and >90% of the cells were positive on ALP staining after osteogenic induction. We also induced these cells to differentiate into multiple lineages by the methods for neural (Kohyama *et al.*, 2001), cardiomyogenic (Makino *et al.*, 1999; Takeda *et al.*, 2004), and chondrogenic (Imabayashi *et al.*, 2003) lineages; however, the UCBMSC and UCBTERT-21 cells were not induced to differentiate into these lineages in vitro.

## DISCUSSION

This study was undertaken to obtain human UCB-derived fetal cells that retain critical cell functions, the same as bone marrow-derived mesenchymal stem cells, mammary gland

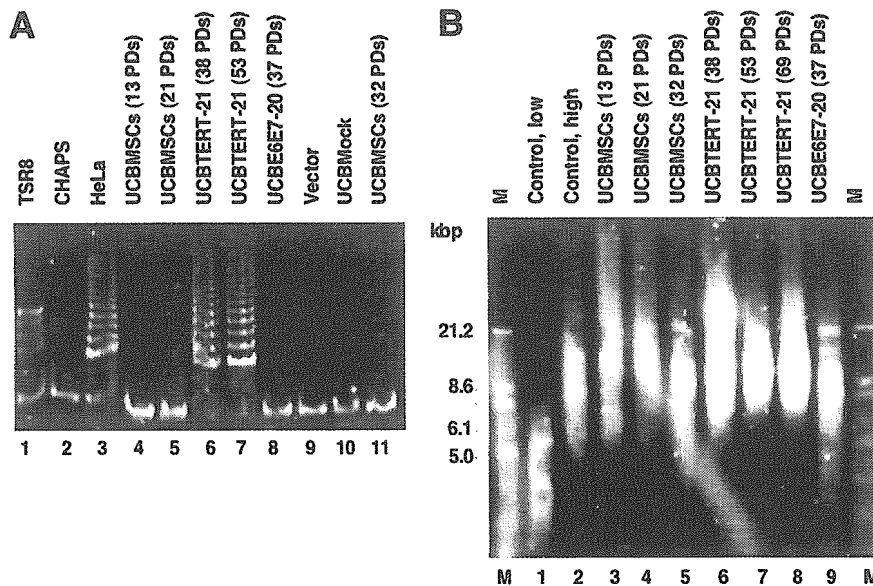


**Figure 4.** Telomerase activity and telomere length of UCBMSCs, UCBE6E7-20 cells, and UCBTERT-21 cells. (A) Analysis of telomerase activity by the PCR assay in UCBMSCs, UCBE6E7-20 cells, and UCBTERT-21 cells. Telomerase activity is revealed by the characteristic six-base pair ladder of bands. No telomerase activity was detected in the UCBMSCs at PD 13, 21, or 32 (lanes 4, 5, and 11, respectively), the UCBE6E7-20 cells at PD 37 (lane 8), the UCBMSCs infected with the vector alone (lane 9), the CHAPS buffer alone (lane 2) or Mock infected cells (lane 10). By contrast, the UCBTERT-21 cells at PD 38 and 53 exhibited significant telomerase activity (lanes 6 and 7, respectively) that was comparable with that of the HeLa cells (lane 3) and TSR8 (lane 1) as positive controls. (B) Telomere length of UCBMSCs, UCBE6E7-20 cells, and UCBTERT-21 cells. Telomere length was longer in the UCBTERT-21 cells than in the parental UCBMSCs. The telomere length of UCBMSCs at PD 13, 21, and 32 decreased as the number of PDs increased (lanes 3–5). The telomere length of UCBTERT-21 cells was maintained, and the telomere length of UCBE6E7-20 cells at PD 37 (lane 9) was shorter than that of the parental UCBMSCs at PD 32 (lane 5). Lanes 1 and 2 are control DNAs of short length and long length, respectively.

irrespective of the number of PDs (lanes 6–8). The telomere length of UCBE6E7-20 cells at PD 37 (lane 9) was shorter than that of the parental UCBMSCs at PD 32 (lane 5). Lanes 1 and 2 are control DNAs of short length and long length, respectively.

epithelial cells, skin keratinocytes, and pigmented epithelial cells. It may be possible to use human UCB- and bone marrow-derived stem cells in the future clinically to supply defective enzymes to patients with genetic metabolic diseases, such as neuro-Gaucher disease, Fabry disease, and mucopolysaccharidosis, whose prognosis is poor, and is sometimes lethal. To achieve this, we attempted to prolong the life span of UCB-derived cells or to endow them with immortality without transformation, defining “immortality” simply as indefinite cell division.

#### *Is Successful Prolongation of UCBMSCs Life Span without Inhibition of the p16<sup>INK4a</sup>/RB Pathway Attributable to a Lack of Ex Vivo Culture Stress?*

In contrast to our previous study by using bone marrow-derived cells (Takeda *et al.*, 2004), surprisingly, the successful prolongation of the life span of the UCB-derived fetal cells obtained in this study did not require inhibition of the p16<sup>INK4a</sup>/RB pathway or premature senescence-associated pathway. Immortalization of some human cell types requires inhibition of the p16<sup>INK4a</sup>/RB pathway in addition to activation of telomerase (Kiyono *et al.*, 1998; Ishikawa, 2003). Human mammary epithelial cells, endometrial glandular cells, skin keratinocytes, and marrow-derived cells require inhibition of the p16<sup>INK4a</sup>/RB pathway for immortalization, but foreskin fibroblasts do not. Activation of telomerase alone is sufficient for immortalization of human foreskin fibroblasts. HPV16 E6 and E7 have been used to inhibit p53 and RB, respectively, to prolong the life span of marrow-derived MSCs (Okamoto *et al.*, 2002; Takeda *et al.*, 2004), endometrial gland cells (Kyo *et al.*, 2003), mammary epithelial cells, and keratinocytes (Kiyono *et al.*, 1998). Bmi-1 also has been used to inhibit p16<sup>INK4a</sup> transcription to prolong the life span of marrow-derived MSCs. One function of this p16<sup>INK4a</sup> protein is to maintain pRB in a hypophosphorylated active form, which inhibits cell cycle progression.

Our present findings that UCB-derived cells can be immortalized without inhibition of the p16<sup>INK4a</sup>/RB pathway is consistent with the results in regard to foreskin fibroblasts. This successful immortalization of UCB-cells by hTERT

alone can be explained by lack of ex vivo culture stress under the culture condition used in this study. Alternatively, only cells insensitive to ex vivo culture stress or lacking p16<sup>INK4a</sup> induction may be expanded by hTERT alone. Primary UCB-derived cell culture succeeded in 94% of the attempts (15 of 16 trials), and the cells were passaged only two or three times before reaching premature senescence (13 of 15 primary UCB-derived cell cultures); however, only two cell strains (UCBMSCs) were established from them (2 of 15 primary UCB-derived cell cultures; see *Materials and Methods*. “Isolation and Cell Culture of UCBMSCs”). Based on the results of this study by using one of the two cell strains, the establishment of these strains (UCBMSCs) can be explained by 1) lack of p16<sup>INK4a</sup> in primary cultured UCB-derived cells or 2) selection of cells that do not express p16<sup>INK4a</sup> from a heterogeneous population. We cannot exclude either possibilities, and we did observe two different types of cells, i.e., rapidly growing cells and quiescent cells in the primary culture of cord blood cells. If the alternative explanation is true, these quiescent cells, in which p16<sup>INK4a</sup> may be expressed at a high level, can be efficiently expanded by introduction of E7, the inhibitor of RB, or Bmi-1, the down-regulator of p16<sup>INK4a</sup>. We also performed additional experiments by using newly obtained specimens from umbilical cord to determine whether infection of the primary or first passage cells generates long-term strains routinely and efficiently. We generated other cells, UCB408 cells, and found that generation of long-term strains was reproducible (Supplementary Figure A). The UCBE6E7-31 and UCBE7-32 cells proliferated for >30 PDs and exhibited persistent growth. The UCBTERT-30 cells exhibited a prolonged cell life span in culture and reached PD 19, but they failed to be immortalized. The success of immortalization of UCBMSCs may still be low, probably due to expression of p16<sup>INK4a</sup> premature senescence-associated proteins in the early passage of the UCB408 cells. Because the 5' CpG island of the p16<sup>INK4a</sup> promoter based on published genome sequences (GenBank accession no. AF022809, U12818, and AC000048) has been found to be methylation-free by the bisulfite method (Supplementary Figures B and C), the lack of